



LJMU Research Online

Viggars, MR, Wen, Y, Peterson, CA and Jarvis, JC

Automated cross-sectional analysis of trained, severely atrophied and recovering rat skeletal muscles using MyoVision 2.0.

<http://researchonline.ljmu.ac.uk/id/eprint/16131/>

Article

Citation (please note it is advisable to refer to the publisher's version if you intend to cite from this work)

Viggars, MR, Wen, Y, Peterson, CA and Jarvis, JC (2022) Automated cross-sectional analysis of trained, severely atrophied and recovering rat skeletal muscles using MyoVision 2.0. Journal of Applied Physiology (1985). ISSN 8750-7587

LJMU has developed [LJMU Research Online](#) for users to access the research output of the University more effectively. Copyright © and Moral Rights for the papers on this site are retained by the individual authors and/or other copyright owners. Users may download and/or print one copy of any article(s) in LJMU Research Online to facilitate their private study or for non-commercial research. You may not engage in further distribution of the material or use it for any profit-making activities or any commercial gain.

The version presented here may differ from the published version or from the version of the record. Please see the repository URL above for details on accessing the published version and note that access may require a subscription.

For more information please contact researchonline@ljmu.ac.uk

<http://researchonline.ljmu.ac.uk/>

1 *Automated cross-sectional analysis of trained, severely atrophied and recovering rat skeletal muscles*
2 *using MyoVision 2.0*

3 Mark R Viggars^{1,2,3*}, Yuan Wen^{4,5,6*}, Charlotte A Peterson^{4,5}, Jonathan C Jarvis¹

4 ¹*Research Institute for Sport and Exercise Sciences, Liverpool John Moores University, Liverpool, UK.*

5 ²*Department of Physiology and Functional Genomics, University of Florida, Gainesville, Florida.*

6 ³*Myology Institute, University of Florida, Gainesville, Florida.*

7 ⁴*Department of Physiology, College of Medicine, University of Kentucky, Lexington, Kentucky.*

8 ⁵*Center for Muscle Biology, University of Kentucky, Lexington, Kentucky.*

9 ⁶*MyoAnalytics, LLC, Lexington, Kentucky.*

10 **Joint First Authors*

11 *Correspondence: Mark Viggars (m.viggars@ufl.edu) Physical Address: ²Department of Physiology and Functional Genomics, University of*
12 *Florida, Gainesville, Florida, USA, 32608.*

13 **Abstract:**

14 The number of myonuclei within a muscle fiber is an important factor in muscle growth, but its
15 regulation during muscle adaptation is not well understood. We aimed to elucidate the timecourse
16 of myonuclear dynamics during endurance training, loaded and concentric resistance training, and
17 nerve silencing-induced disuse atrophy with subsequent recovery. We modified tibialis anterior
18 muscle activity in free-living rats with electrical stimulation from implantable pulse generators, or
19 with implantable osmotic pumps delivering tetrodotoxin (TTX) to silence the motor nerve without
20 transection. We used the updated, automated software MyoVision to measure fiber type-specific
21 responses in whole tibialis anterior cross-sections (~8000 fibers each). Seven days of continuous low
22 frequency stimulation (CLFS) reduced muscle mass (-12%), increased slower myosin isoforms and
23 reduced IIX/IIB fibers (-32%) and substantially increased myonuclei especially in IIX/IIB fibers
24 (55.5%). High load resistance training (Spillover), produced greater hypertrophy (~16%) in muscle
25 mass and fiber cross-sectional area (CSA) than low load resistance training (concentric, ~6%) and was
26 associated with myonuclear addition in all fiber types (35-46%). TTX-induced nerve silencing resulted
27 in progressive loss in muscle mass, fiber CSA, and myonuclei per fiber cross-section (-50.7%, -53.7%,
28 -40.7%, respectively at 14 days). Myonuclear loss occurred in a fiber type-independent manner, but
29 subsequent recovery during voluntary habitual activity suggested that type IIX/IIB fibers contained
30 more new myonuclei during recovery from severe atrophy. This study demonstrates the power and

31 accuracy provided by the updated MyoVision software and introduces new models for studying
32 myonuclear dynamics in training, detraining, retraining, repeated disuse, and recovery.

33 **New & Noteworthy**

34 We introduce new models for studying fiber-type specific myonuclear dynamics in muscle training,
35 detraining, retraining, disuse, and recovery. We show that the various fiber types do not respond
36 identically, and that myonuclear number changes during adaptation. We also critically assess an
37 updated version of MyoVision automated image analysis software, to quantify whole muscle
38 immunofluorescent microscopical images in a faster and less computer intensive manner. MyoVision
39 remains open source and freely available with more user-controlled features.

40 **Introduction:**

41 Skeletal muscle is highly responsive to changes in mechanical forces. Additional load is a key
42 regulator of muscle hypertrophy, and muscle unloading is a trigger for muscle atrophy (1). There are
43 several potential adaptive mechanisms that may allow trained muscle to recover faster than
44 untrained muscle from periods of catabolism including epigenetic modifications (2, 3) and/or miRNA
45 levels and myonuclear shape (4). Myonuclear number itself has also been suggested as a potentially
46 stable indicator of previous episodes of hypertrophy (5). Myonuclei can alter their transcriptional
47 activity in response to mechanical cues, such as those caused by exercise, as well as to internal
48 factors such as proximity to other myonuclei (6-9). Increase in synthetic activity following exercise
49 probably reflects a shift in mRNA expression to reprogram cellular phenotype in response to the
50 demands imposed on the muscle fiber, as well as increasing rRNA expression to increase
51 translational efficiency and capacity (6, 10, 11).

52 To support transcriptional demands during muscle remodelling, it may be necessary to increase the
53 number of myonuclei per unit cell volume. Since muscle fibers are post-mitotic, this is achieved
54 through muscle stem cells (satellite cells), which can proliferate and then fuse to myofibers adding

55 new myonuclei. The presence of satellite cells is not completely obligatory for short term load-
56 induced hypertrophy (12), or androgen-induced hypertrophy (13), but in adult skeletal muscle (14),
57 their depletion alters the myonuclear transcriptome and blunts adaptation to exercise,
58 proprioception and exercise capacity (15-17). Satellite cells also play an important role in muscle
59 homeostasis by communicating with endothelial and fibroadipogenic progenitor cells in skeletal
60 muscle, as well as with the myonuclei themselves (18-21). However, whether all nuclei or newly
61 added myonuclei are permanent and able to act as a cellular memory (5), or whether they can be
62 lost through caspase dependent and caspase-independent (Endonuclease G) mechanisms is yet to
63 be fully confirmed (22).

64 Training followed by subsequent 'detraining' has revealed that different individual muscles show a
65 variety of responses. Six months of detraining after 2 months of progressive weighted wheel running
66 (PoWeR) showed that the fiber type shifts, fiber hypertrophy and increases in myonuclear number
67 caused by training were reversed after detraining in the gastrocnemius and plantaris muscles (4, 23).
68 By contrast, the soleus muscle did not lose PoWeR adaptations following detraining and type I fibers
69 showed higher myonuclear content with no increase in fiber size. Clearly, the loss or addition of
70 myonuclei following training and detraining is a complicated phenomenon with the data indicating
71 that there are large differences between responses according to training model, species, age, muscle
72 group and muscle fiber type (24). How muscle disuse compares with detraining and whether
73 recovery from disuse atrophy is comparable to training-induced hypertrophy in terms of myonuclear
74 dynamics are currently unknown. The requirement for new myonuclei and whether those nuclei are
75 retained may be controlled by a combination of motor activity, oxidative capacity, and tonic stretch.

76 Currently, the most direct and accurate methods to assess myonuclei number are myonuclear
77 counts in single extracted myofibers, or intravital imaging of the small number of myonuclei visible
78 in superficial fibers (7, 25-28). However, these methods are labor intensive and may not represent
79 the population of myonuclei within a muscle with typically thousands to tens of thousands of fibers

80 with complex architectural properties, different resting/working lengths, and differing activation
81 patterns. Thus, assessing entire whole muscle cross-sections via immunohistochemical labelling as
82 we have done here remains the most accessible and unbiased approach if performed by automatic,
83 high throughput image analysis.

84 In this investigation, we combined the improved capabilities of MyoVision automated histological
85 analysis software to characterize adaptive changes in myonuclei number per fiber on whole cross-
86 sections of tibialis anterior, each containing between 6000 and 10,000 fibers, in 3 adaptive
87 conditions: 1) A time course of programmed daily resistance exercise: high load contractions,
88 achieved by a technique we call 'Spillover stimulation' because the supramaximal stimulation of the
89 common peroneal nerve is adjusted to 'spill over' to activate some of the antagonistic motor units of
90 the plantarflexors supplied by the tibial nerve) vs. unloaded contractions (concentric) to induce
91 hypertrophy, 2) continuous low frequency stimulation (CLFS) to induce an endurance-trained
92 phenotype and 3) disuse atrophy by means of reversible nerve silencing with subsequent recovery
93 (29, 30). Our objective for each paradigm of muscle adaptation was to understand changes in cross
94 sectional area for each fiber type and whether this correlated with myonuclear content. We
95 hypothesized that following our exercise training protocols, as all muscle fibers are activated
96 synchronously, the extent of growth and myonuclear accretion may reflect the total activity
97 time/loading similarly in all fiber types. Furthermore, as our atrophy model prevents propagation of
98 action potentials in all muscle fibers, myonuclei might be lost in a fiber type-independent manner,
99 but the recovery by habitual voluntary activity might produce myonuclear accretion according to the
100 normal graded recruitment of muscle fibers.

101 **Methods:**

102 *Experimental Design*

103 The animal experiments were conducted under the provisions of the Animals (Scientific Procedures)
104 Act 1986 and approved by the British Home Office (PPL 40/3280). Male Wistar rats were group-

105 housed with 2-3 per cage maintaining an alternating 12 h light 12 h dark cycle. The mean age of all
106 rats was 18 ± 2 weeks upon euthanasia. All animals survived their elected experimental timecourse.
107 Pre-surgical and post experimental weights for each group can be found in Table 2.

108

109 INSERT TABLE 2 HERE

110 INSERT FIGURE 1 HERE

111 *Resistance Training Protocols & Pattern*

112 Animals received 1 session per day of high load (Spillover) or low load (concentric) resistance
113 training (RT) in the left hind-limb via stimulation from an implanted pulse generator (IPG) as
114 previously described (30), for 2 ($n=4$), 10 ($n=6$), 20 ($n=6$), or 30 days ($n=8$), or underwent sham
115 surgery ($n=6$). Briefly, for high load (Spillover) exercise to elicit slight stretch under load, the
116 dorsiflexor muscles, tibialis anterior (TA) and extensor digitorum longus (EDL), received
117 supramaximal activation via a cathode placed underneath the common peroneal nerve (CPN), while
118 the anode was positioned underneath the tibial nerve. Stimulation current was adjusted by remote
119 programming, to recruit enough of the gastrocnemius, plantaris and soleus (plantarflexor muscles)
120 to provide appropriate resistance against the contraction of the dorsiflexors. In an additional group
121 ($n=6$), animals received 1 session per day of unresisted (concentric) contractions of the dorsiflexors
122 for 30 days by placing both electrodes under the CPN during implantation so there was no activation
123 of the plantarflexor muscles, and the dorsiflexors contracted against a low load.

124 Daily training was delivered during the first hour of the inactive light phase automatically by the IPG
125 and consisted of an initial 10 seconds of preparatory stimulation at a low frequency ($F = 4\text{Hz}$, phase
126 width = $258 \mu\text{s}$, current = approximately 1 mA), followed by 5 sets of 10 tetanic contractions at 100
127 Hz. Each contraction lasted for 2s with 2s rest between contractions and 2.5 minutes of rest
128 between sets. The stimulation was delivered only in the left hind-limb, so muscles of the right hind-

129 limb acted as unstimulated contralateral controls. Stimulation with these settings and the amplitude
130 chosen to balance dorsiflexion and plantarflexion described above was well-tolerated by all animals
131 without further anaesthesia or sedation. Regular observations during daily training across the time
132 course revealed no adverse behavioural signs.

133 Continuous Low Frequency Stimulation (CLFS)

134 As previously described (29, 31), the ankle dorsiflexors of the left hind-limb were continuously
135 stimulated (24 h per day), at 20Hz for 7 days ($n=6$). This pattern has previously been shown to induce
136 a transformation from the control fast phenotype towards a slower more oxidative phenotype in the
137 dorsiflexor muscles characteristic of endurance training (32).

138 Electrical Stimulation Surgical Procedure

139 Animals were anaesthetised during implant procedures by inhalation of a gaseous mixture of
140 isoflurane in oxygen at approximately 3% for induction and 1-2% for maintenance. Once
141 anaesthetised, a subcutaneous injection of Enrofloxacin ($5\text{mg}/\text{kg}^{-1}$ body mass (Baytril®) and an
142 intramuscular injection of Buprenorphine ($0.05\text{mg}/\text{kg}^{-1}$ body mass) (Temgesic, Indivior, Slough, UK)
143 into the right quadriceps was administered with strict asepsis maintained throughout the procedure.
144 Nerve stimulation was delivered from silicone-encapsulated implanted pulse generators (IPGs)
145 (MiniVStim 12B, Competence Team for Implanted Devices, Center for Medical Physics and
146 Biomedical Engineering, Medical University Vienna, Austria) which could be programmed remotely
147 by a radio frequency link. The devices were implanted into the abdominal cavity accessed by a
148 lateral incision through the skin and peritoneum, between the rib cage and pelvis on the left side of
149 the animal. A polyester mesh attached to the IPG was incorporated into the suture line closing the
150 peritoneum, securing the device against the abdominal wall. Two PVC-insulated stainless-steel
151 electrode leads (Cooner Sales Company, Chatsworth, California, U.S.A.) with terminal conductive
152 loops, were fed through the peritoneal incision and tunnelled under the skin to the lateral side of the
153 upper left hind-limb. A second incision was made through the skin and biceps femoris muscle to give

154 access to the CPN under which the cathode was placed (to stimulate the dorsiflexors). The anode
155 was either placed alongside the cathode to stimulate the CPN alone and thus to produce unresisted
156 (concentric) contractions or placed in the muscular tissue deep to the tibial nerve about 5mm distal
157 to its bifurcation from the sciatic nerve to allow Spillover stimulation to produce additional partial
158 activation of the plantarflexors to resist the contraction of the dorsiflexors, resulting in a loaded
159 contraction. All incisions were closed in layers and 3-7 days were allowed for recovery from surgery
160 before the start of the training protocol. Once programmed, the stimulators ran autonomously to
161 provide the selected activation pattern over the course of the experiment.

162 *Nerve Silencing-Induced Disuse by Tetrodotoxin & Recovery Protocols*

163 INSERT FIGURE 2 HERE

164 The CPN, the motor nerve responsible for contraction of the TA and EDL, was silenced with
165 tetrodotoxin (TTX) for pre-set periods of 3 days ($n=4$), 7 days ($n=6$), or 14 days ($n=6$). Atrophy of the
166 dorsiflexors was produced without signs of fiber necrosis or denervation assessed by H&E staining. A
167 separate group was used to assess recovery after 14 days of tetrodotoxin (TTX) treatment. Osmotic
168 pumps were appropriately loaded so that the TTX infusion was exhausted after 14 days, and nerve
169 activity could resume during 7 days of muscle recovery via habitual physical activity ($n=6$). Pumps
170 were weighed before implantation and again after explant to confirm that the expected volume of
171 TTX had been delivered over the time course of the experiment. Muscle mass data from these
172 groups has previously been reported (29).

173 *Tetrodotoxin Administration Surgical Procedure*

174 Animals were anaesthetised as previously described for the implantable stimulator surgeries. A
175 miniosmotic pump (Mini Osmotic Pump 2002; Alzet, Cupertino, CA, USA) was implanted
176 subcutaneously in the scapular region. Silicone tubing was tunnelled under the skin to the site of the
177 CPN. A second incision was made laterally through the skin, just proximal to the knee joint and bicep

178 femoris muscle (posterior compartment of the thigh) in order to give access to the CPN responsible
179 for action of the dorsiflexors. A silicone cuff extending from the silicone tubing was placed around
180 the nerve. All incisions were closed in layers. The miniosmotic pump (Mini Osmotic Pump 2002;
181 Alzet, Cupertino, CA, USA) delivered TTX, a sodium channel blocker that prevents generation and
182 propagation of action potentials at the CPN of the left hind-limb. The osmotic pump successfully
183 delivered 0.5 μ l/h TTX (350mg/ml in sterile 0.9% saline), continuously blocking ankle dorsiflexion,
184 while maintaining normal voluntary plantarflexion via the tibial nerve. Disuse of the dorsiflexors by
185 this means produces progressive atrophy (29). The welfare and mobility of the rats was checked
186 daily by animal welfare staff. There was little disturbance to mobility, but sometimes 'foot drop' was
187 observed, a gait abnormality characterised by dropping of the forefoot due to the inhibition of
188 dorsiflexion.

189 Rat muscle sampling and preservation

190 Animals were humanely sacrificed using rising concentrations of carbon dioxide (at a displacement
191 rate of 50% of the animals' home cage volume per minute), followed by cervical dislocation. TA
192 muscles from both hind limbs were immediately harvested, cleaned of excess connective tissue, and
193 weighed. The mid-belly of the TA was cut out, placed on cork for transverse sectioning and frozen in
194 melting isopentane above liquid nitrogen for later immunohistochemical analysis.

195 Immunohistochemistry

196 Muscle samples were sectioned at 10 μ m using an OTF5000 Cryostat (Bright Instruments, UK) onto
197 Thermo Scientific™ SuperFrost Plus™ Adhesion slides (Thermo Fisher Scientific Inc, Waltham, USA).
198 Muscle cross-sections were labelled with primary antibodies against dystrophin (MANDYS8-8H11 or
199 a polyclonal dystrophin antibody (1:200)) to demarcate the inside of the sarcolemma for all the
200 experimental samples. Fiber type analysis was performed on TA muscles within the 30 days loaded
201 RT, 30 days concentric RT, 7 days 20Hz CLFS, 14 days atrophy and 14 days atrophy with 7 days
202 recovery groups, through labelling of dystrophin, as well as BA-D5 (anti myosin type I) and SC-71

203 (anti myosin type IIA) hybridoma supernatants (1:100), diluted in immunobuffer (IB) overnight and
204 then washed 3 x 10 minutes in IB. Unstained muscle fibers were later measured as IIX/IIB fibers.
205 Appropriate secondary antibodies with specific Ig fragments were diluted in IB for 2 hours (1:500),
206 followed by 3 x 10 minutes in IB. IB consists of 50mM glycine (Merck 1.02401_1000), 0.25% BSA,
207 0.03% saponin (Sigma 100g S-7900), and 0.05% sodium azide in phosphate buffered saline (PBS,
208 10mM phosphate pH 7.4, 150mM NaCl).

209 For all cross-sections, following incubation with primary and secondary antibodies (Table 1), nuclei
210 were labelled with DAPI (D1306, Thermofisher Scientific) at a concentration of 30nM diluted in PBS
211 for 30 minutes, prior to 3 x 5-minute washes in PBS. Coverslips were then mounted onto cross-
212 sections with VECTASHIELD® Antifade Mounting Medium (Vector Laboratories, UK). Hematoxylin
213 and Eosin (H&E) staining was also performed on serial or 'near serial' sections within ~10-60µm, to
214 check for evidence of damage, de/regeneration and fiber loss by independent researchers.

215 Table 1: Primary antibodies and appropriate corresponding secondary antibodies used.

216 INSERT TABLE 1 HERE

217

218 Imaging

219 Once labelled, whole muscle cross-sections were imaged using a widefield fluorescent microscope
220 (Leica DMB 6000, Wetzlar, Germany) with a 10x objective. Multiple images were automatically
221 stitched together using the tilescan feature in the Leica Application Suite.

222 MyoVision 2.0 Analysis:

223 MyoVision 2.0 introduced major upgrades to the original MyoVision software, but the fundamental
224 workflow including fiber detection, fiber type classification, and myonuclear counting remained
225 essentially the same as described previously (33). For fiber detection, the software uses the single

226 channel intensity image of dystrophin labelling as an input as well as the pixel scale ($\mu\text{m}/\text{pixel}$) to
227 allow for calculation of mean fiber cross-sectional area in units of square micrometres. Following
228 fiber detection, a single channel intensity image of immuno-labelled myosin heavy chain or nuclei
229 can be provided to the software to classify fiber type or quantify myonuclei number. For each
230 myofiber cytoplasmic region excluding the periphery, the mean myosin heavy chain
231 immunofluorescence intensity was quantified on a scale of 0 to 1, with 1 being maximum signal for
232 the section. Only fibers with mean myosin heavy chain intensity greater than 0.5 were classified as
233 true for that particular fiber type. When analysing multiple fiber types, the image corresponding to
234 each fiber type staining was analysed independently. Thus, a fiber classified as “negative” would
235 represent false for all fiber types included in the analysis whereas a “hybrid” classification would
236 indicate co-expression of at least two different myosin heavy chain isoforms within the same fiber.
237 The criteria for myonuclear classification remain the same as in the previous version; specifically, a
238 nuclear region with its centroid inside the fiber dystrophin border and at least 50% of its total area
239 within the fiber cytoplasm is counted as a myonucleus.

240 A major upgrade to the software is the implementation of neural networks in fiber detection and
241 fiber type classification steps. As summarized in Supplementary Figure 1, multiple steps in the
242 previous MyoVision algorithm have been replaced with U-net models (34), which demonstrated
243 superior performance in the segmentation of grayscale intensity based images of cells. The models
244 were trained using annotated images of 256 by 256 pixels. Briefly, images of whole cross-sections
245 were labelled as true for foreground (i.e. fiber boundary) and false for background (i.e. non-specific
246 signals or staining artefacts). These images along with their ground truth label were separated into
247 256x256 pixel regions. The same image and ground truth label were then reduced by two-fold in size
248 sequentially, and 256x256 pixel regions were extracted from the smaller images in a similar fashion
249 as the original image. Reducing the image size allows for the model to learn at different image
250 resolutions and different magnifications. Images representing 1x, 0.5x, and 0.25x along with their
251 ground truth labels were used to train the weights of a U-net model for up to 100 epochs at 300

252 steps per epoch using Keras (v2.2.4) and Tensorflow (v1.13.1). Models were similarly trained for
253 each step in the algorithm to replace the corresponding steps in the previous version of the software
254 (Supplementary Figure 1). Of note, the previous software included the active contour algorithm by
255 default, which expands the fiber contour as close to the inner edge of the dystrophin border as
256 possible to allow for myonuclear counting. The previous version included a step that separated
257 (shrank) certain cytoplasmic regions that were probably connected; thus, the active contour
258 algorithm was applied to every fiber outline to expand the contour of the cytoplasmic space to the
259 inner edge of the dystrophin border. This step had been relocated to the nuclear counting analysis
260 exclusively due to its resource intensiveness and the fact that general fiber detection does not
261 require such stringent delineation of the inner edge of the sarcolemma. This modification led to the
262 same fiber cross-sectional area values, but a reduction in the defined 'cytoplasmic region' which is
263 now slightly smaller (~5%) than the value estimated by the previous version of the software. This
264 modification was favorable not only from a computational resource perspective, but also resulted in
265 values more in line with various other approaches in the literature that do not include any
266 myonuclear analysis. The software will be made freely available to the research community and
267 additional documentation for the current version can be found on
268 www.myoanalytics.com/myovision2. Together these modifications make it possible to analyse
269 much larger images than was possible on the previous version of MyoVision and improve the access
270 for the user to the calculated data for every fiber recognised in the image.

271 In addition, users now have control over circularity, solidity and eccentricity parameters for
272 identifying fibers (Supplementary Figure 2), for analysis of different muscle phenotypes and extreme
273 atrophic conditions. Other functionalities introduced in this upgrade include robust detection of
274 whole cross-sections, batch processing of images for large projects, export of representative images
275 from the software, exporting images from Olympus microscopes, adjusting images to control for
276 background noise, and output of multiple shape descriptors for each fiber.

277 A total of 166 complete cross-sections of rat TA were generated by tile scanning and reconstructing
278 to generate single image files for each muscle in our test and control groups. These were analyzed in
279 the process of beta testing of the new software taking an average of 29.80 ± 4.87 minutes per cross-
280 section for detection and analysis of fiber CSA, three fiber types and myonuclear number on a PC
281 Specialist laptop, equipped with an Intel® Core™ i7-6700K CPU 4.00GHz processor and 64GB of RAM.
282 Use of a CUDA-capable GPU having a Compute Capability of greater than 3.5 and 8GB or more
283 dedicated memory would further increase the speed of image processing and analysis.

284 Manual Quantification versus Myovision 2.0 for assessing severely atrophied muscle fibers

285 Hematoxylin and Eosin (H&E) stained cross-sections were used for manual quantification of fiber
286 number, which was performed on 5 self-selected fields of view containing (~450-600) muscle fibers
287 with the most severe atrophy after 14 days of TTX treatment. Using the multi-point tool in Image-Pro
288 Plus 5.1 software (Media Cybernetics, MD, USA), fiber number was counted and then compared with
289 analysis by Myovision of the serial immunohistochemically labelled field of view, identified by means
290 of landmarks such as blood vessels or distinctive connective tissues.

291 Statistics

292 Data are presented as the % change between the left experimental hind-limb and right internal
293 contralateral control hind-limb for overall muscle mass (mg/kg bodyweight), fiber CSA, myonuclei
294 per fiber cross-section and myonuclear domain across all experimental models, that is, the absolute
295 difference (positive or negative) expressed as a percentage of the control value. The resultant
296 percentage changes were then compared via one-way ANOVA, followed by Tukey's post-hoc analysis
297 to confirm differences between groups. For fiber type-specific analysis, absolute values of fiber
298 number, fiber type proportion, fiber CSA, myonuclei per fiber cross-section and myonuclear domain
299 were compared between groups using one-way ANOVA's, followed by Tukey's post-hoc analysis to
300 confirm differences between groups. Simple linear regression was also performed on % changes
301 between muscle mass, fiber CSA, myonuclei per fiber cross-section and myonuclear domain size. For

302 the recovery group from TTX, co-efficient of variation was performed on values produced by
303 expressing the 14 days TTX with 7-day recovery muscle values, as a percentage change from the
304 mean 14-day TTX treatment values to show the extent of myonuclear addition as a % increase,
305 rather than a % decrease from baseline. Significance was set at $P < 0.05$ for all statistical analyses,
306 performed in GraphPad Prism 9.0 software. All data are presented as mean \pm standard deviation
307 (SD).

308 **Results:**

309 *Tibialis anterior (TA) fiber type, number, size and myonuclear characteristics in control hind-limbs*

310 We first sought to assess the fiber type composition, fiber cross-sectional area (CSA) and
311 myonuclear-related characteristics of the rat TA muscle in 32 untreated control hind-limbs across all
312 our experimental conditions. Although the TA is a predominately fast-twitch muscle, we pay
313 particular attention to the more oxidative, slower myosin isoform-containing muscle fibers as they
314 still make up approximately 25% of all muscle fibers at the mid-belly and therefore have functional
315 significance. We note that myosin heavy chain profiles can change across the length of a muscle, and
316 we only study the mid-belly, other longitudinal regions should be considered dependent on the
317 muscle. Our data (Figure 3A) confirms previous measurements of fiber type percentages in rat TA
318 with IIX/IIB fibers ($75.7 \pm 8.4\%$) representing a significantly higher population than all other
319 measured fiber types ($P < 0.00001$). While IIA fibers represented a significantly lower proportion of
320 the TA muscle ($21.29 \pm 7.1\%$), they represented a significantly higher proportion than type I/IIA
321 hybrids ($3.09 \pm 2.4\%$, $P = < 0.0001$) or pure type I fibers ($2.04 \pm 1.1\%$, $P = < 0.0001$), respectively. There
322 was no significant difference between the proportion of type I and type I/IIA hybrid fibers, $P = 0.859$.
323 As well as being the predominant fiber types in the TA, type IIX/IIB fibers also possess significantly
324 higher mean fiber CSA ($2380 \pm 327 \mu\text{m}^2$) than all other fiber types measured (Figure 3B), $P < 0.00001$.
325 Type IIA mean fiber CSA ($1399 \pm 212 \mu\text{m}^2$), was significantly larger than both type I/IIA hybrid fiber
326 CSA ($1158 \pm 208 \mu\text{m}^2$, $P = 0.0010$) and type I fiber CSA ($1180 \pm 229 \mu\text{m}^2$, $P = 0.0053$). Furthermore,

327 there was no significant difference between type I/IIA hybrids and type I fiber CSA. Interestingly,
328 there was no significant difference between any of the fiber types for the number of myonuclei per
329 fiber cross-section (Figure 3C), with type I, I/IIA hybrids, IIA, and IIX/IIB fibers containing 0.96 ± 0.2 ,
330 1.01 ± 0.22 , 1.09 ± 0.22 , 1.03 ± 0.23 myonuclei per cross-section, respectively. As a result,
331 myonuclear domain size, that is average cross-sectional area per nucleus, was significantly larger in
332 type IIX/IIB fibers ($2564 \pm 1742\mu\text{m}^2$) than all other fiber types measured, $P < 0.0001$ (Figure 3D).
333 There was no significant difference between type I ($1417 \pm 620\mu\text{m}^2$), type I/IIA hybrids ($1483 \pm$
334 $727\mu\text{m}^2$) and type IIA ($1362 \pm 544\mu\text{m}^2$) myonuclear domain sizes. The mean total fiber number
335 detected across all control TAs ($n=32$) was 8060 ± 1078 per TA (Figure 3E). Despite a large sample
336 size, co-efficient of variation (CV) was still 13.38% for total fiber number, demonstrating the need for
337 an internal contralateral control measurement. The CV of the difference in fiber number between
338 left and right hind-limbs is only 5.04% from 63 pairs of TAs in this study. Total fiber number was not
339 significantly different between any group or between the left experimental TA and right internal
340 contralateral control TA after any treatment ($P > 0.05$) (Figure 3E). Some variation was present
341 between left and right hind-limbs in the same animal which we believe is a combination of natural
342 fiber number variation between contralateral limbs.

343 INSERT FIGURE 3 HERE.

344 Continuous low frequency stimulation (CLFS) of the TA induced a reduction in fiber CSA, an increase in
345 myonuclear content and changes in myosin heavy chain isoform composition.

346 As a model of endurance training, we applied CLFS to the TA unilaterally and used the contralateral
347 leg as a control. To check that surgical intervention alone did not alter muscle mass, fiber CSA or
348 myonuclear characteristics, sham IPGs and electrodes were implanted in the left hind-limb, and
349 animals given 7 days to recover before euthanasia and muscle assessment. There were no significant
350 differences in any characteristics studied between the operated and contralateral control TA in this
351 sham group (Figure 4A-D). By contrast, 7 days of 24 hours per day 20Hz stimulation caused a

352 significant decrease in muscle mass ($-12.6 \pm 4.86\%$, $P = 0.0026$) (Figure 4A) in comparison to the
353 unoperated control TA, concomitant with a similar decrease in muscle fiber CSA ($-18.59 \pm 11.41\%$, P
354 $= 0.024$), Figure 4B). Despite the loss in mass and fiber CSA, there was a highly variable yet significant
355 increase in myonuclei per fiber ($53.44 \pm 44.87\%$, $P = 0.0328$, Figure 4C) when assessed across the
356 entire muscle cross-section, resulting in a significantly lower myonuclear domain size (-56.08 ± 27.87
357 $\%$, $P = 0.0097$, Figure 4D).

358 When assessing fiber type-specific changes, there was a shift in fiber type proportion (Figure 4E-G)
359 with a significant reduction in IIX/IIB fibers from $80.5 \pm 8.4\%$ to $62 \pm 11.3\%$, $P = 0.0003$ after 7 days of
360 CLFS. The percentage of type I ($2.09 \pm 1.6\%$ vs. $4.95 \pm 2.95\%$, $P = 0.99$) and IIA fibers ($15.65 \pm 6.75\%$
361 vs. $15.53 \pm 2.9\%$, $P = 0.99$) did not alter significantly between control and CLFS limbs respectively,
362 although there was a substantial increase in Type I/IIA hybrids following CLFS ($1.78 \pm 1.8\%$ to $17.52 \pm$
363 8.2% , $P = 0.0032$) suggesting that IIX/IIB fibers had shifted to IIA and existing IIA fibers had shifted to
364 a type I/IIA hybrid phenotype. Interestingly, there were no significant differences in fiber CSA (Type I
365 Control, $1357 \pm 225\mu\text{m}^2$ vs. Type I CLFS, $1252 \pm 100\mu\text{m}^2$, $P = 0.99$. Type I/IIA hybrid control $1201 \pm$
366 $370\mu\text{m}^2$ vs. Type I/IIA hybrid CLFS $1061 \pm 160\mu\text{m}^2$, $P = 0.97$. Type IIA Control $1370 \pm 141\mu\text{m}^2$ vs. Type
367 IIA CLFS $1316 \pm 157\mu\text{m}^2$, $P = 0.99$. Type IIX/IIB control $2253 \pm 371\mu\text{m}^2$ vs. Type IIX/IIB CLFS $1954 \pm$
368 $312\mu\text{m}^2$, $P = 0.45$ (Figure 4H-J), despite the overall significant decrease in muscle fiber CSA ($-18.59 \pm$
369 11.41% , $P = 0.024$). Therefore, the transformation of IIX/IIB to IIA myosin isoforms is probably the
370 combined effect of insignificant decreases in fiber size, as well as a shift in fiber type proportion
371 (Figure 4E-G).

372 To further elucidate the significant increase in myonuclei per fiber across the entire muscle cross-
373 section following CLFS, we analysed myonuclei per fiber cross-section for each fiber type. While
374 there were trends suggesting addition of myonuclei in Type I (0.88 ± 0.15 vs. 1.06 ± 0.16 , $P = 0.83$,
375 Figure 4K), Type I/IIA hybrid (0.94 ± 0.06 vs. 1.1 ± 0.16 , $P = 0.85$, Supplementary Figure 3C), and Type
376 IIA (0.94 ± 0.19 vs. 1.26 ± 0.23 , $P = 0.14$, Figure 4L) fibers, the increase in the mean value only

377 reached significance in IIX/IIB fibers (0.85 ± 0.23 vs. 1.32 ± 0.31 , $P = 0.0044$, Figure 4M). This was
378 further reflected in the sizes of the myonuclear domain, which was significantly reduced only in the
379 IIX/IIB fibers ($3990 \pm 2554 \mu\text{m}^2$ vs. $1232 \pm 394 \mu\text{m}^2$, $P = 0.0007$, Figure 4P).

380 INSERT FIGURE 4 HERE

381 *Loaded resistance training (Spillover) produces a greater hypertrophic and myonuclear response than*
382 *concentric resistance training.*

383

384 Loaded RT produced a $3.3 \pm 1.6\%$ change in muscle mass after just 2 days of stimulation ($P = 0.1$) and
385 reached statistical significance after 10 days ($13.6 \pm 5.8\%$, $P = < 0.0001$), 20 days ($16.7 \pm 4.4\%$, $P =$
386 < 0.0001) and 30 days ($15.9 \pm 5.6\%$, $P = < 0.0001$), in comparison to both sham surgery ($P < 0.001$)
387 and their contralateral internal controls ($P < 0.001$) (Figure 5A). There were no significant differences
388 between 10, 20 and 30 days of loaded RT, illustrating that muscle mass had plateaued between 10
389 and 20 days and thus, further daily training did not increase muscle mass. Thirty days of training with
390 the identical daily activation but no active resistance from the plantar flexors produced a significant
391 increase in muscle mass ($6.2 \pm 4.5\%$, $P = 0.05$), but was significantly lower than with 10, 20 or 30
392 days of loaded RT ($P = 0.0493$, $P = 0.0036$ and $P = 0.0037$, Figure 5A). Analysing overall changes in
393 muscle fiber CSA revealed a delayed increase compared to muscle mass (Figure 5B), with a trend
394 suggesting an increase in fiber CSA after 20 days vs the sham control group ($7.61 \pm 1.58\%$, $P = 0.316$),
395 which reached significance after 30 days vs. the sham control group ($17.55 \pm 8.56\%$, $P = < 0.0001$).
396 Concentric RT did not cause a significant increase in fiber CSA vs the sham control group ($5.19 \pm$
397 2.23% , $P = 0.78$), meaning that 30 days loaded RT showed significantly higher increases in CSA than
398 30 days of concentric RT ($P = 0.0019$). Part of the early increases in mass may be due to muscle
399 swelling, and the lack of a plateau in the CSA data suggests that fiber hypertrophy is ongoing even
400 after 30 days of loaded RT. Similarly, myonuclei per fiber cross-section did not significantly increase
401 after 2 and 10 days but showed a trend to increase after 20 days ($35.29 \pm 21.18\%$, $P = 0.1948$, Figure

402 5C) and reached significance after 30 days of loaded RT ($54.59 \pm 42.64\%$, $P = 0.0041$), which was also
403 significantly higher than the 30-day concentric RT group ($11.89 \pm 10.06\%$, $P = 0.0255$, Figure 5C).

404

405 After identifying significant increases in both muscle mass, fiber CSA and myonuclei per fiber cross-
406 section after 30 days of loaded RT, but no significant changes in anything but muscle mass after 30
407 days of concentric RT, we sought to identify any potential fiber type-specific adaptations at the 30
408 days timepoint. There were no significant changes in fiber type proportion, but we note fiber-type
409 specific changes in size in response to loaded and concentric RT modalities, despite identical activity
410 patterns and activation of all fibers simultaneously during stimulation. 30 days of loaded RT
411 produced a significant increase in type I fiber CSA above the control group ($1507 \pm 261\mu\text{m}^2$ vs. $1105 \pm$
412 $241\mu\text{m}^2$, $P = 0.0031$), whereas 30 days of concentric RT was not significantly different between the
413 control and 30-day loaded RT group. ($1273 \pm 73.9\mu\text{m}^2$, $P > 0.907$), (Figure 5H). While fiber CSA
414 seemed to be observably higher in some animals, large variation in the training groups meant there
415 were no significant differences between Type I/IIA hybrid fibers between control ($1149 \pm 188\mu\text{m}^2$)
416 and both 30 days of loaded ($1359 \pm 307\mu\text{m}^2$, $P = 0.558$), or 30 days of concentric RT ($1302 \pm 95\mu\text{m}^2$, P
417 $= 0.9474$, Supplementary Figure 4B). Although modest trends appeared, no significant differences
418 were detected in Type IIA fibers between control fiber CSA ($1392 \pm 154\mu\text{m}^2$), and both 30 days of
419 loaded ($1650 \pm 265\mu\text{m}^2$, $P = 0.236$), or 30 days of concentric RT ($1522 \pm 135\mu\text{m}^2$, $P = 0.984$), (Figure
420 5I). By contrast, a robust increase in Type IIX/IIB fiber CSA was observed between the control and 30
421 days of loaded RT (2481 ± 222 vs. $2969 \pm 268\mu\text{m}^2$, $P < 0.0001$), which was not observed after 30 days
422 of concentric RT ($2673 \pm 176\mu\text{m}^2$, $P = 0.795$, Figure 5J).

423

424 Myonuclei per fiber cross-section was significantly higher across all fiber types studied after 30 days
425 of loaded RT vs control: Type I (1.43 ± 0.26 vs. 1.023 ± 0.16 , $P = 0.0078$, Figure 5K); Type I/IIA hybrids
426 (1.28 ± 0.35 vs. 0.93 ± 0.14 , $P = 0.023$, Supplementary Figure 4C); Type IIA (1.5 ± 0.31 vs. $1.047 \pm$
427 0.17 , $P = 0.0015$, Figure 5L); and Type IIX/IIB (1.448 ± 0.36 vs. 1.062 ± 0.24 , $P = 0.0161$, Figure 5M). By

428 contrast, with concentric training, we only observed modest trends suggesting that myonuclei were
429 added after 30 days but none reached significance (Type I, 1.23 ± 0.16 , $P = 0.823$. Type I/IIA Hybrids,
430 1.28 ± 0.18 , $P = 0.11$. Type IIA, 1.31 ± 0.22 , $P = 0.46$. Type IIX/IIB, 1.39 ± 0.21 , $P = 0.18$), (Figure 5M-
431 P). Despite this, there were no significant differences between myonuclei per fiber after 30 days
432 loaded and 30 days concentric RT (Type I, $P = 0.89$. Type I/IIA Hybrids, $P = 0.98$ Type IIA, $P = 0.93$.
433 Type IIX/IIB, $P = 0.98$). Furthermore, there were no significant differences in myonuclear domain size
434 across any of the fiber types investigated between the control and both loaded and concentric 30-
435 day training groups (Figure 5N-P), suggesting that myonuclei were added in proportion to the
436 increase in fiber CSA.

437

438 Using simple linear regression analysis to assess the relationships between measured variables
439 across our timecourse of RT, we found significant positive correlations between percent changes in
440 muscle mass and percent changes in fiber CSA ($R^2 = 0.2324$, $P = <0.007$) and myonuclei per fiber
441 cross-section ($R^2 = 0.1568$, $P = 0.0303$, Figure 7A-B). The co-efficient of variation between percent
442 changes in muscle mass and percent change in myonuclear domain size was not significant, ($R^2 =$
443 0.08682 , $P = 0.114$, Figure 7C). Percent change in fiber CSA had a significant positive correlation with
444 percent change in myonuclei per fiber cross-section ($R^2 = 0.3826$, $P = 0.0003$) and had a positive
445 trend toward significance with the percent change in myonuclear domain size ($R^2 = 0.1214$, $P =$
446 0.0592 , Figure 7D-E). As expected, the co-efficient of variation for percent change in myonuclear
447 domain size and percent change in myonuclei per fiber cross-section reached significance ($R^2 =$
448 0.8137 , $P = <0.0001$, Figure 7F).

449

INSERT FIGURE 5 HERE

450 *TTX-induced skeletal muscle disuse atrophy causes a loss of myonuclei, and subsequent recovery of*
451 *muscle mass is associated with substantial myonuclear addition.*

452

INSERT FIGURE 6 HERE

453 As previously reported (29), exposure to TTX produced a progressive loss in TA muscle mass of -6.98
454 $\pm 2.5\%$ at 3 days, $-29.4 \pm 5\%$ at 7 days and $-50.7 \pm 2.9\%$ after 14 days. The changes were significant at
455 all time points vs. the sham operated group, -0.03 ± 2.5 ($P < 0.0001$), (Figure 6A). After 14 days of
456 TTX exposure, followed by 7 days of recovery by habitual activity, muscle mass significantly
457 recovered by 51.7% vs. 14 days of TTX exposure ($P < 0.001$). Seven days of recovery did not
458 completely restore muscle mass, as muscle mass was still significantly lower than the sham group (P
459 < 0.001), although muscle mass was not significantly different to the 7 days of TTX administration
460 group ($P = 0.56$), which suggests that the rate of loss over 7 days is similar to the rate of recovery.
461 We made a completely new immunohistochemical analysis for this paper, cutting new sections from
462 the same frozen muscles for analysis of whole muscle cross-sections with the updated MyoVision
463 software. A trend was observed, suggesting a loss in detected fibers after 14 days atrophy of $-19.5 \pm$
464 7.8% , ($P=0.052$). However, when fiber number was manually counted on hematoxylin and eosin
465 (H&E) stained tissue sections from 14-day TTX treatment, looking specifically at the most severely
466 atrophied fibers, there was good agreement with the automatic detection in the most challenging
467 fields of view, ($87.7 \pm 4.3\%$), where $\sim 13\%$ of the fibers had become too small or squashed to be
468 successfully identified by MyoVision as a muscle fiber as opposed to interstitial tissue. With
469 MyoVision 2.0, we added a feature for users to change the myofiber identification parameters in
470 relation to circularity, solidity, and eccentricity to allow for adjustment to muscle phenotypes where
471 cross-sectioned fibers become less round (more pennate architecture) and may be not identified
472 based on default parameters (Supplementary Figure 2). However, for our analyses we kept the
473 default parameters the same for consistency across experimental groups (0.6 circularity, 0.85
474 solidity, 0.95 eccentricity).

475 H&E staining showed no evidence of fiber loss, splitting or newly formed fibers in any of our multiple
476 endpoints as previously reported (29, 30). Muscle fiber CSA progressively declined vs. the sham
477 operated group, reaching significance at 7 days ($-33.7 \pm 9.2\%$, $P < 0.0001$) and further declining at 14
478 days ($-53.7 \pm 10.8\%$, $P < 0.0001$). After cessation of TTX delivery and 7 days recovery, muscle fiber

479 CSA was still significantly lower than the sham operated group ($P = 0.012$), despite significantly
480 increasing ($-20.4 \pm 11.1\%$) vs. the 14-day atrophy timepoint. Much like muscle mass, fiber CSA losses
481 were not significantly different to the 7 days atrophy timepoint ($P = 0.293$), suggesting CSA
482 recovered at the same rate as CSA loss (Figure 6B).

483 Measurements of myonuclei per fiber cross-sectional area revealed a trend suggesting myonuclei
484 were being progressively lost after only 7 days of atrophy ($-26.2 \pm 21\%$, $P = 0.45$), later reaching
485 significance after 14 days of atrophy ($-40.72 \pm 21\%$, $P = 0.0489$). From the substantial loss of
486 myonuclei per fiber cross-section observed after 14 days of atrophy ($-40.72 \pm 21\%$), 7 days of
487 recovery allowed for myonuclei per fiber cross-section to significantly increase by $38.67 \pm 33.08\%$ vs.
488 their internal contralateral controls ($P = 0.049$). This suggests that myonuclei are added in substantial
489 numbers above baseline values to aid in the regrowth of muscle following atrophy, (Figure 6C).
490 Myonuclear domain size % changes did not differ significantly between any of the time points,
491 (Figure 6D).

492

493 To identify whether the changes in myonuclear content varied between fiber types, we conducted
494 further analyses on the 14-day atrophy group and 14-day atrophy with 7 days recovery group.
495 Analysis of fiber type proportions at both timepoints revealed no significant differences in overall
496 fiber type percentage, though a trend was observed for an increase in type IIA fibers after 14 days of
497 atrophy ($32.72 \pm 8.07\%$, $P = 0.357$) and 14 days of atrophy with 7 days recovery ($34 \pm 12.04\%$, $P =$
498 0.118) vs. the control limbs ($24.43 \pm 6.12\%$), (Figure 6E-G). This was concomitant with trends
499 suggesting a reduction in type IIX/IIB fibers after 14 days atrophy ($60.86 \pm 10.14\%$, $P = 0.2153$), and
500 following subsequent recovery ($59.04 \pm 13.44\%$, $P = 0.0575$) versus the control group ($70.01 \pm 6.19\%$)
501 (Figure 6G).

502

503 With no clear shifts in fiber type, we assessed fiber CSA to determine whether atrophy was similar
504 across fiber types. The shape of the bar charts looks similar for each fiber type, but significant

505 differences were only noted in type IIA and IIX/B fibers. In comparison to the control type I fibers
506 ($1179 \pm 178\mu\text{m}^2$), 14 days of TTX treatment did not cause a significant decrease in fiber CSA ($796 \pm$
507 $170\mu\text{m}^2$, $P = 0.14$), nor a significant change in the recovery group ($988 \pm 155\mu\text{m}^2$), from either the
508 control ($P = 0.94$), or atrophied muscles ($P = 0.98$, Figure 6H). Similarly, type I/IIA hybrids ($1148 \pm$
509 $130\mu\text{m}^2$) showed no significant decline following atrophy ($796 \pm 125\mu\text{m}^2$, $P = 0.24$), or recovery from
510 atrophy ($1009 \pm 72\mu\text{m}^2$, $P = 0.957$, Supplementary Figure 5B). However, there was a significant
511 decrease in type IIA fiber CSA after 14 days ($1423 \pm 298\mu\text{m}^2$ vs. $968 \pm 89\mu\text{m}^2$, $P = 0.035$), which had
512 recovered back to the mean control CSA after recovery ($1368 \pm 77\mu\text{m}^2$, $P = 0.99$, Figure 6I). By
513 contrast, while type IIX/IIB fiber CSA was reduced by 56.6% in the atrophy group ($2325 \pm 394\mu\text{m}^2$ vs.
514 $1010 \pm 228\mu\text{m}^2$, $P < 0.0001$), fiber CSA was not able to recover completely to the level of the control
515 muscle after 7 days of recovery ($1746 \pm 601\mu\text{m}^2$, $P = 0.0016$), although this was significantly higher
516 than the 14 days of atrophy timepoint ($P = < 0.0001$, Figure 6J).

517

518 Assessment of myonuclei per fiber cross-section in type I fibers revealed no differences between the
519 control TA (0.93 ± 0.25) and the 14-day atrophy group (1.11 ± 0.24 , $P = 0.96$), or the 14-day atrophy
520 with 7 days of recovery group (0.86 ± 0.29 , $P = 0.99$), (Figure 6K). Myonuclei per fiber cross-section in
521 type I/IIA hybrid fibers revealed a significant reduction in myonuclei (1.16 ± 0.24 vs. 0.71 ± 0.17 , $P =$
522 0.0219), but recovered back to control levels after just 7 days (1.23 ± 0.31 , $P = 0.99$), and was
523 significantly higher than the 14-day atrophy timepoint ($P = 0.0239$) for this fiber type
524 (Supplementary Figure 5C). A similar trend was observed in type IIA fibers which lost myonuclei after
525 14 days of atrophy (1.2 ± 0.26 vs. 0.68 ± 0.26 , $P = 0.0046$), but recovered after 7 days (1.16 ± 0.3 , $P =$
526 0.05) to the extent that there was no significant difference from the control group ($P = 0.99$), (Figure
527 6L). While myonuclei number in the type IIX/IIB fiber was significantly reduced after the atrophy
528 period compared to the control group (1.09 ± 0.18 vs. 0.61 ± 0.08 , $P = 0.01$), myonuclei number per
529 fiber cross-section significantly increased in the recovery group (1.68 ± 0.34), both above the 14 days
530 atrophy group ($P = < 0.0001$) and surprisingly further beyond the control group ($P = 0.0005$), (Figure

531 6M). We then assessed whether the myonuclear domain size was therefore altered following
532 substantial atrophy and found no significant differences in type I ($P > 0.3$), type I/IIA hybrid ($P > 0.98$),
533 or type IIA ($P > 0.90$) fibers, between the control, atrophy, and atrophy with recovery groups, (Figure
534 6N-P). However, a trend was detected in type IIX/IIB fibers, suggesting a decrease in domain size
535 between the control and 14-day atrophy group ($2232 \pm 731 \mu\text{m}^2$ vs. $1664 \pm 310 \mu\text{m}^2$, $P = 0.285$). A
536 significantly lower myonuclear domain size was detected between the control TAs and the 14-day
537 atrophy with 7-day recovery group ($970 \pm 241 \mu\text{m}^2$, $P < 0.0001$), (Figure 6P).

538

539 Linear regression analysis revealed a significant positive correlation between percent change in
540 muscle mass and percent change in fiber CSA ($R^2 = 0.8589$, $P = < 0.0001$), percent change in
541 myonuclei per fiber cross-section ($R^2 = 0.8589$, $P = < 0.0001$) and percent change in myonuclear
542 domain size ($R^2 = 0.4550$, $P = 0.0008$, Figure 7G-I). There were also significant positive correlations
543 between percent change in fiber CSA and both percent change in myonuclei per fiber cross-section
544 ($R^2 = 0.8079$, $P = < 0.0001$) and percent change in myonuclear domain size ($R^2 = 0.5439$, $P = 0.0001$,
545 Figure 7J-K). The co-efficient of variation between the percent change in myonuclei per fiber cross-
546 section and percent change in myonuclear domain size was also significant ($R^2 = 0.2468$, $P = 0.022$,
547 Figure 7L).

548 **Discussion:**

549 In both developing and adult mammalian skeletal muscle, myonuclei number, often referred to as
550 DNA content, varies with muscle fiber size although this relationship is not completely linear, nor is it
551 fully understood in all contexts of muscle plasticity (7, 24, 35). Our objective was to understand the
552 fiber type specific changes in cross-sectional area and whether this correlated with changes in
553 myonuclear content in our models of growth, endurance training, atrophy and recovery. We
554 developed MyoVision as the first unbiased, fully automatic software that is freely available to the
555 muscle research community, and since then, there has been significant interest in such analytical

556 packages for muscle cross-sections (36-41). Despite the overall interest, MyoVision remains one of
557 only two freely available programs that include myonuclear quantification and the only one for
558 which this function is validated. A major limitation of MyoVision was its computational inefficiency
559 that precluded analysis of large cross-sections, such as the whole rat TA, taken at high magnification.
560 In most instances, the previous version of the software would not successfully analyse such large
561 images, but the new software provides this capability through improved computational speed and
562 efficiency. Additionally, MyoVision analysis was previously sensitive to background noise, which
563 increased the requirement on microscope image quality. To address these shortcomings, we have
564 updated MyoVision and optimized the software to allow for rapid and unsupervised quantification of
565 hundreds of thousands of individual myofibers and millions of nuclei on histological cross-sections
566 (www.myoanalytics.com/myovision2).

567 CLFS for 7 days which mimics endurance training caused a significant reduction in mean muscle mass
568 ($-12.6 \pm 4.9\%$, $P = 0.0026$), mean fiber CSA ($-18.6 \pm 11.4\%$, $P = 0.024$) and a shift from glycolytic to
569 smaller, more oxidative fibers (type IIX/IIB fiber percentage fell from 81% to 62%). There were no
570 changes in fiber CSA when assessed at the fiber type level (Figure 4H-J), suggesting that the larger
571 IIX/IIB fibers that shifted myosin heavy chain content also reduced their fiber area which may be an
572 adaptation to reduce the diffusion distance to allow increased respiratory gas exchange associated
573 with a shift to oxidative metabolism (42-46). Myonuclear addition is generally considered to be a
574 feature of resistance exercise-induced hypertrophy, as a mechanism to support both repair of
575 damaged muscle fibers unaccustomed to exercise (4, 47) and to support transcription across a larger
576 area of cytoplasm (35, 48, 49). However, we found significant increases in myonuclei per fiber cross-
577 section especially in type IIX/IIB glycolytic fibers in response to CLFS. As mean fiber area did not
578 change, IIX/IIB myofiber cytoplasm became hypernucleated per fiber cross-section, so that there was
579 a significant reduction in myonuclear domain size (-69% , $P = 0.0007$), which was closer to the value
580 for oxidative fibers in control muscle.

581 We then studied the fiber type specific effects of RT using spillover (loaded) contractions and high-
582 frequency concentric contractions. While loading from the antagonistic muscle group differs
583 between our RT modalities, our model avoids the complication of variable recruitment among fiber
584 types during the exercise intervention. This allowed us to directly compare the differences in loading
585 on fiber type specific adaptations so that the total volume of activation can be excluded as a factor
586 for differences between fiber types in terms of exercise induced myonuclear accretion. Thirty days
587 of loaded RT caused significantly larger increases in muscle mass, fiber CSA and myonuclear
588 accretion than 30 days of concentric RT, similarly to Eftestøl and colleagues who used a non-surgical
589 model to exercise rat dorsiflexor muscles using transcutaneous electrical stimulation with external
590 load applied through the use of a resisting footplate (50). They reported that higher load was
591 associated with greater fiber hypertrophy and greater myonuclear accretion but did not assess fiber
592 type specific effects. In our loaded RT model after 30 days, fiber area increased significantly in type I
593 fibers by a mean of 36% (Figure 5H) and by a mean of only 19% in type IIX/IIB fibers (Figure 5J).
594 While this increase is somewhat larger in the slow muscle fibers, the relatively small proportion of
595 type I fibers (<6%) and large proportion of IIX/IIB fibers means that IIX/IIB contribute more to whole
596 muscle fiber hypertrophy. However, this is an interesting observation of the potential functional
597 significance of hypertrophy of small populations of slow fibers in a predominantly fast twitch muscle
598 during hypertrophy. Furthermore, myonuclear accretion was similar across all fiber types (Figure 5K-
599 M), suggesting that the accretion of myonuclei is strongly associated with load and activity in this
600 instance. It has previously been argued that slower fibers are more susceptible to exercise-induced
601 damage but this can often be explained by their greater activation in voluntary movement, being
602 recruited to a larger extent than fast oxidative and fast glycolytic fibers (51, 52). Despite this, a
603 recent study in mice using a voluntary exercise on a high load resistance wheel, produced
604 myonuclear accretion in a load dependent manner in the plantarflexor muscles of mice, and the
605 addition of myonuclei occurred similarly across all fiber types (53). In contrast, progressive weighted
606 wheel running (PoWeR) in mice results in both fiber type-specific and fiber type-independent

607 adaptations that differ based on the muscle studied (4). This probably reflects differences in
608 activation and load during voluntary exercise, as well as early damage-related fusion of satellite cells
609 which has previously been reported after unaccustomed exercise (47, 54, 55).

610 Myonuclear loss or maintenance during muscle disuse is of particular interest since the signals
611 related to exercise and load are reduced. Previously, the relationship between muscle loss during
612 disuse in rodents has been performed using injury to the nerve/denervation (25, 56, 57) and hind-
613 limb unloading (22, 58, 59), although the latter model does not control for motor activity, and in
614 some instances it can even be increased, while the load is reduced (60, 61). The use of TTX to study
615 muscle atrophy has been less widely adopted (25, 29, 62, 63). However, TTX nerve treatment causes
616 muscle atrophy through prevention of generation or propagation of action potentials in the nerve,
617 without axonal damage so disuse can be followed by a period of recovery. Trophic factors
618 dependent on axon integrity may continue to have influence on their associated muscle fibers, while
619 substantial sarcoplasm is lost within the muscle fibers (29, 64, 65).

620 As we have previously reported (29), onset of TTX treatment causes a progressive loss in muscle
621 mass and mean fiber CSA reaching significance after 7 days and further declining at 14 days (Figure
622 6A-B). Our new fiber-type specific analysis shows that this is mainly attributed to significant loss of
623 CSA in type IIA (-47%) and IIX/IIB fibers (-56%) (Figure 6I-J) while simultaneously reducing myonuclei
624 per fiber cross-section in both IIA and IIX/IIB fibers (43%), therefore maintaining myonuclear domain
625 size. Intriguingly, type I fibers did not atrophy significantly, and they maintained their myonuclei
626 number. Similar treatment involving the entire sciatic nerve for 2 weeks found that type IIA muscle
627 fibers atrophied less (29%) than type IIB fibers (43%) in the TA of rats (63). Sciatic nerve block also
628 prevents activity of the plantarflexors; it was observed that the lateral gastrocnemius IIB and IIA
629 fibers showed less atrophy (23-26%) than the resident type I fibers (44%), but in the soleus, both fast
630 and slow fibers atrophied to the same extent (39% versus 43%). Differences in the rates and total
631 extent of muscle atrophy have been reported between different muscles and different fiber types

632 which may be related to oxidative capacity, protein synthetic/degradation rates and the resting
633 length of the muscle (63, 66, 67). Only one study to our knowledge has measured myonuclei number
634 in response to TTX treatment, although this was performed in mice. Intravital imaging showed no
635 decrease in myonuclei with intravital imaging after 3 weeks in the EDL muscle which may be related
636 to species differences or the fact that the EDL crosses two joints and therefore has a higher level of
637 passive tension, perhaps enough to prevent loss of myonuclei.

638 During the 7-days recovery post TTX treatment, muscle mass significantly recovered by 51.7% versus
639 14 days of TTX exposure ($P < 0.001$). Type IIA fibers recovered fiber CSA and myonuclei per fiber
640 cross-section measurements in line with control levels during this period. This recovery was not
641 matched in the less oxidative type IIX/IIB fibers which had only partially recovered their CSA from 14
642 days of nerve silencing ($P = 0.003$). Remarkably, myonuclei per fiber cross-section was higher in
643 comparison to both the atrophied muscle ($P = <0.0001$) and the control muscle ($P = 0.0005$) in IIX/IIB
644 fibers, suggesting that myonuclear populations did not only recover back to the point of baseline,
645 but were also added past homeostatic levels to support the substantial recovery of muscle mass and
646 fiber CSA from severe atrophy, somewhat like resistance exercise-induced myonuclear accretion.
647 This resulted in hypernucleated type IIX/IIB fibers, versus their control counterparts. We also
648 observed this characteristic in our CLFS model, suggesting that due to type IIX/IIB fibers having larger
649 myonuclear domains than their slower, more oxidative counterparts under control conditions, they
650 may be more dependent on myonuclear accretion to support the changes in activity or periods of
651 regrowth. It is of significant interest whether type IIX/IIB fibers retain the extra myonuclei added
652 during the recovery from TTX-induced atrophy or whether they are lost as muscle returns to basal
653 mass, so that they act as 'temporary' myonuclei to support the rapid growth. Or, if they are retained
654 how this would affect subsequent periods of unloading and future periods of growth.

655 **Future Considerations:**

656 The use of IPGs allows for programming and control over both endurance and resistance exercise so
657 that training duration, contraction modality, repetitions, sets, rest and the timing of exercise within
658 the circadian cycle can all be prescribed. IPGs can be easily programmed to switch on or off allowing
659 for periods of detraining and subsequent retraining with minimal intervention or use of
660 supraphysiological methods. Analogously, the careful planning and loading of osmotic pumps to
661 deliver TTX to a motor nerve allows for periods of disuse induced atrophy and subsequent recovery.
662 The replacement of the osmotic pump or use of programmable infusion pumps would also allow for
663 continuous cycling of nerve block and recovery to simulate repeated bed rest in humans. Further
664 functions are continually being added to the automated image analysis program, MyoVision
665 www.myoanalytics.com/myovision2, including guidance on supported image file types and minimum
666 recommended computer requirements.

667 **Conclusion:**

668 We propose that the number of myonuclei is not fixed, probably reflects the changes in activity
669 requirements of the muscle fiber and does not always correlate with fiber size. The myonuclear
670 domain appears highly flexible and adaptations often differ by fiber type. High load RT resulted in
671 increased muscle size associated with higher myonuclear content per muscle fiber, whereas low-
672 load continuous stimulation increased myonuclear content but reduced muscle fiber size. TTX-
673 induced nerve silencing caused atrophy and myonuclear loss, but both were restored with recovery
674 of activity. The recovery in type IIX/IIB fibers includes an over compensatory addition of myonuclei
675 to the muscle fiber. Overall, our models of high load short duration and low load continuous
676 stimulation, and recovery after disuse all resulted in substantial increases in myonuclei without
677 histological signs of muscle damage as assessed by histology.

678 **Supplementary Figures 1-5**

679 <https://doi.org/10.6084/m9.figshare.17904347> (Supplementary File 1, Supplementary Figures 1-2).

680 <https://doi.org/10.6084/m9.figshare.16775677> (Supplementary File 2, Supplementary Figures 3-5).

681 **Acknowledgments:**

682 The authors thank Dr Hazel Sutherland for expert help with the implant operations and muscle
683 harvesting.

684 The authors thank Dr. Kevin Murach for his discussions and useful insights on the manuscript.

685 **Author Contributions:**

686 M.V, J.C.J designed experiments. M.V, J.C.J performed experiments. Y.W and M.V analyzed and
687 interpreted data. Y.W. built the updated software. M.V and Y.W. wrote the manuscript and prepared
688 figures with the support and review of J.C.J and C.A.P.

689 **Declaration of interests:**

690 In the past year, Y.W. has worked as a consultant for the Core Muscle Research laboratory at the
691 University of Alabama and he declares ownership in MyoAnalytics, LLC.

692 **References:**

- 693 1. **Schiaffino S, Dyar KA, Ciciliot S, Blaauw B, and Sandri M.** Mechanisms regulating skeletal
694 muscle growth and atrophy. *The FEBS journal* 280: 4294-4314, 2013.
- 695 2. **Sharples AP, Polydorou I, Hughes DC, Owens DJ, Hughes TM, and Stewart CE.** Skeletal
696 muscle cells possess a 'memory' of acute early life TNF- α exposure: role of epigenetic adaptation.
697 *Biogerontology* 17: 603-617, 2016.
- 698 3. **Seaborne R, Strauss J, Cocks M, Shepherd S, O'Brien T, Van Someren K, Bell P, Murgatroyd**
699 **C, Morton J, and Stewart C.** Methylome of human skeletal muscle after acute & chronic resistance
700 exercise training, detraining & retraining. *Scientific data* 5: 1-9, 2018.
- 701 4. **Murach KA, Mobley CB, Zdunek CJ, Frick KK, Jones SR, McCarthy JJ, Peterson CA, and**
702 **Dungan CM.** Muscle memory: myonuclear accretion, maintenance, morphology, and miRNA levels
703 with training and detraining in adult mice. *Journal of cachexia, sarcopenia and muscle* 2020.
- 704 5. **Gundersen K.** Muscle memory and a new cellular model for muscle atrophy and
705 hypertrophy. *Journal of Experimental Biology* 219: 235-242, 2016.
- 706 6. **Joplin R, Franchi L, and Salmons S.** Changes in the size and synthetic activity of nuclear
707 populations in chronically stimulated rabbit skeletal muscle. *Journal of anatomy* 155: 39, 1987.
- 708 7. **Cramer AA, Prasad V, Eftestøl E, Song T, Hansson K-A, Dugdale HF, Sadayappan S, Ochala J,**
709 **Gundersen K, and Millay DP.** Nuclear numbers in syncytial muscle fibers promote size but limit the
710 development of larger myonuclear domains. *Nature communications* 11: 1-14, 2020.

- 711 8. Kirby TJ, Patel RM, McClintock TS, Dupont-Versteegden EE, Peterson CA, and McCarthy JJ.
712 Myonuclear transcription is responsive to mechanical load and DNA content but uncoupled from cell
713 size during hypertrophy. *Molecular biology of the cell* 27: 788-798, 2016.
- 714 9. Windner SE, Manhart A, Brown A, Mogilner A, and Baylies MK. Nuclear scaling is
715 coordinated among individual nuclei in multinucleated muscle fibers. *Developmental Cell* 49: 48-62.
716 e43, 2019.
- 717 10. Goldspink DF, Cox VM, Smith SK, Eaves LA, Osbaldeston NJ, Lee DM, and Mantle D. Muscle
718 growth in response to mechanical stimuli. *American Journal of Physiology-Endocrinology And*
719 *Metabolism* 268: E288-E297, 1995.
- 720 11. Nader GA, McLoughlin TJ, and Esser KA. mTOR function in skeletal muscle hypertrophy:
721 increased ribosomal RNA via cell cycle regulators. *American Journal of Physiology-Cell Physiology*
722 2005.
- 723 12. McCarthy JJ, Mula J, Miyazaki M, Erfani R, Garrison K, Farooqui AB, Srikuea R, Lawson BA,
724 Grimes B, and Keller C. Effective fiber hypertrophy in satellite cell-depleted skeletal muscle.
725 *Development* 138: 3657-3666, 2011.
- 726 13. Englund DA, Peck BD, Murach KA, Neal AC, Caldwell HA, McCarthy JJ, Peterson CA, and
727 Dupont-Versteegden EE. Resident muscle stem cells are not required for testosterone-induced
728 skeletal muscle hypertrophy. *American Journal of Physiology-Cell Physiology* 317: C719-C724, 2019.
- 729 14. Murach KA, White SH, Wen Y, Ho A, Dupont-Versteegden EE, McCarthy JJ, and Peterson
730 CA. Differential requirement for satellite cells during overload-induced muscle hypertrophy in
731 growing versus mature mice. *Skeletal muscle* 7: 1-13, 2017.
- 732 15. Goh Q, Song T, Petrany MJ, Cramer AA, Sun C, Sadayappan S, Lee S-J, and Millay DP.
733 Myonuclear accretion is a determinant of exercise-induced remodeling in skeletal muscle. *Elife* 8:
734 e44876, 2019.
- 735 16. Englund DA, Murach KA, Dungan CM, Figueiredo VC, Vechetti Jr IJ, Dupont-Versteegden
736 EE, McCarthy JJ, and Peterson CA. Depletion of resident muscle stem cells negatively impacts
737 running volume, physical function and muscle hypertrophy in response to lifelong physical activity.
738 *American Journal of Physiology-Cell Physiology* 2020.
- 739 17. Englund DA, Figueiredo VC, Dungan CM, Murach KA, Peck BD, Petrosino JM, Brightwell CR,
740 Dupont AM, Neal AC, and Fry CS. Satellite cell depletion disrupts transcriptional coordination and
741 muscle adaptation to exercise. *Function* 2: zqaa033, 2021.
- 742 18. Verma M, Asakura Y, Murakonda BSR, Pengo T, Latroche C, Chazaud B, McLoon LK, and
743 Asakura A. Muscle satellite cell cross-talk with a vascular niche maintains quiescence via VEGF and
744 notch signaling. *Cell stem cell* 23: 530-543. e539, 2018.
- 745 19. Madaro L, Mozzetta C, Biferali B, and Proietti D. Fibro-Adipogenic Progenitors (FAPs) cross-
746 talk in skeletal muscle: the social network. *Frontiers in physiology* 10: 1074, 2019.
- 747 20. Murach KA, Vechetti Jr IJ, Van Pelt DW, Crow SE, Dungan CM, Figueiredo VC, Kosmac K, Fu
748 X, Richards CI, and Fry CS. Fusion-independent satellite cell communication to muscle fibers during
749 load-induced hypertrophy. *Function* 1: zqaa009, 2020.
- 750 21. Murach KA, Peck BD, Policastro RA, Vechetti IJ, Van Pelt DW, Dungan CM, Denes LT, Fu X,
751 Brightwell CR, and Zentner GE. Early satellite cell communication creates a permissive environment
752 for long-term muscle growth. *Iscience* 24: 102372, 2021.
- 753 22. Dupont-Versteegden EE, Strotman BA, Gurley CM, Gaddy D, Knox M, Fluckey JD, and
754 Peterson CA. Nuclear translocation of EndoG at the initiation of disuse muscle atrophy and
755 apoptosis is specific to myonuclei. *Am J Physiol Regul Integr Comp Physiol* 291: R1730-1740, 2006.
- 756 23. Dungan CM, Murach KA, Frick KK, Jones SR, Crow SE, Englund DA, Vechetti Jr IJ, Figueiredo
757 VC, Levitan BM, and Satin J. Elevated myonuclear density during skeletal muscle hypertrophy in
758 response to training is reversed during detraining. *American Journal of Physiology-Cell Physiology*
759 316: C649-C654, 2019.
- 760 24. Snijders T, Aussieker T, Holwerda A, Parise G, van Loon LJ, and Verdijk LB. The concept of
761 skeletal muscle memory: Evidence from animal and human studies. *Acta Physiologica* e13465, 2020.

762 25. **Bruusgaard JC, and Gundersen K.** In vivo time-lapse microscopy reveals no loss of murine
763 myonuclei during weeks of muscle atrophy. *The Journal of clinical investigation* 118: 1450-1457,
764 2008.

765 26. **Stewart MD, Jang CW, Hong NW, Austin AP, and Behringer RR.** Dual fluorescent protein
766 reporters for studying cell behaviors in vivo. *genesis* 47: 708-717, 2009.

767 27. **Hastings RL, Massopust RT, Haddix SG, Lee Yi, and Thompson WJ.** Exclusive vital labeling of
768 myonuclei for studying myonuclear arrangement in mouse skeletal muscle tissue. *Skeletal Muscle*
769 10: 1-13, 2020.

770 28. **Hansson K-A, Eftestøl E, Bruusgaard JC, Juvkam I, Cramer AW, Malthe-Sørensen A, Millay
771 DP, and Gundersen K.** Myonuclear content regulates cell size with similar scaling properties in mice
772 and humans. *Nature communications* 11: 1-14, 2020.

773 29. **Fisher AG, Seaborne RA, Hughes TM, Gutteridge A, Stewart C, Coulson JM, Sharples AP,
774 and Jarvis JC.** Transcriptomic and epigenetic regulation of disuse atrophy and the return to activity in
775 skeletal muscle. *The FASEB Journal* 31: 5268-5282, 2017.

776 30. **Schmoll M, Unger E, Sutherland H, Haller M, Bijak M, Lanmüller H, and Jarvis JC.** SpillOver
777 stimulation: A novel hypertrophy model using co-contraction of the plantar-flexors to load the tibial
778 anterior muscle in rats. *PLOS ONE* 13: e0207886, 2018.

779 31. **Jarvis J, and Salmons S.** A family of neuromuscular stimulators with optical transcutaneous
780 control. *Journal of medical engineering & technology* 15: 53-57, 1991.

781 32. **Jarvis JC.** Power production and working capacity of rabbit tibialis anterior muscles after
782 chronic electrical stimulation at 10 Hz. *The Journal of Physiology* 470: 157-169, 1993.

783 33. **Wen Y, Murach KA, Vechetti Jr IJ, Fry CS, Vickery C, Peterson CA, McCarthy JJ, and
784 Campbell KS.** MyoVision: software for automated high-content analysis of skeletal muscle
785 immunohistochemistry. *Journal of Applied Physiology* 124: 40-51, 2018.

786 34. **Ronneberger O, Fischer P, and Brox T.** U-net: Convolutional networks for biomedical image
787 segmentation. In: *International Conference on Medical image computing and computer-assisted
788 intervention* Springer, 2015, p. 234-241.

789 35. **Karlsen A, Couppé C, Andersen JL, Mikkelsen UR, Nielsen RH, Magnusson SP, Kjaer M, and
790 Mackey AL.** Matters of fiber size and myonuclear domain: does size matter more than age? *Muscle
791 & nerve* 52: 1040-1046, 2015.

792 36. **Mayeuf-Louchart A, Hardy D, Thorel Q, Roux P, Gueniot L, Briand D, Mazeraud A, Bouglé A,
793 Shorte SL, and Staels B.** MuscleJ: a high-content analysis method to study skeletal muscle with a
794 new Fiji tool. *Skeletal muscle* 8: 1-11, 2018.

795 37. **Encarnacion-Rivera L, Foltz S, Hartzell HC, and Choo H.** Myosoft: an automated muscle
796 histology analysis tool using machine learning algorithm utilizing Fiji/ImageJ software. *PloS one* 15:
797 e0229041, 2020.

798 38. **Lau YS, Xu L, Gao Y, and Han R.** Automated muscle histopathology analysis using CellProfiler.
799 *Skeletal muscle* 8: 1-9, 2018.

800 39. **Waisman A, Norris AM, Costa ME, and Kopinke D.** Automatic and unbiased segmentation
801 and quantification of myofibers in skeletal muscle. *Scientific Reports* 11: 1-14, 2021.

802 40. **Kastenschmidt JM, Ellefsen KL, Mannaa AH, Giebel JJ, Yahia R, Ayer RE, Pham P, Rios R,
803 Vetrone SA, and Mozaffar T.** QuantiMus: a machine learning-based approach for high precision
804 analysis of skeletal muscle morphology. *Frontiers in physiology* 10: 1416, 2019.

805 41. **Sertel O, Dogdas B, Chiu CS, and Gurcan MN.** Microscopic image analysis for quantitative
806 characterization of muscle fiber type composition. *Computerized Medical Imaging and Graphics* 35:
807 616-628, 2011.

808 42. **Brown MD, Cotter MA, Hudlická O, and Vrbová G.** The effects of different patterns of
809 muscle activity on capillary density, mechanical properties and structure of slow and fast rabbit
810 muscles. *Pflügers Archiv* 361: 241-250, 1976.

- 811 43. **Egginton S, and Hudlicka O.** Early changes in performance, blood flow and capillary fine
812 structure in rat fast muscles induced by electrical stimulation. *The Journal of physiology* 515: 265-
813 275, 1999.
- 814 44. **Hudlicka O, Brown M, Cotter M, Smith M, and Vrbova G.** The effect of long-term
815 stimulation of fast muscles on their blood flow, metabolism and ability to withstand fatigue. *Pflügers*
816 *Archiv* 369: 141-149, 1977.
- 817 45. **Hudlicka O, Dodd L, Renkin E, and Gray S.** Early changes in fiber profile and capillary density
818 in long-term stimulated muscles. *American Journal of Physiology-Heart and Circulatory Physiology*
819 243: H528-H535, 1982.
- 820 46. **Hudlická O, Egginton S, and Brown M.** Capillary diffusion distances-their importance for
821 cardiac and skeletal muscle performance. *Physiology* 3: 134-138, 1988.
- 822 47. **Mackey AL, and Kjaer M.** The breaking and making of healthy adult human skeletal muscle
823 in vivo. *Skeletal muscle* 7: 24, 2017.
- 824 48. **Karlsen A, Soendenbroe C, Malmgaard-Clausen NM, Wagener F, Moeller CE, Senhaji Z,**
825 **Damberg K, Andersen JL, Schjerling P, and Kjaer M.** Preserved capacity for satellite cell proliferation,
826 regeneration, and hypertrophy in the skeletal muscle of healthy elderly men. *The FASEB Journal* 34:
827 6418-6436, 2020.
- 828 49. **Snijders T, Holwerda AM, van Loon LJ, and Verdijk LB.** Myonuclear content and domain size
829 in small versus larger muscle fibres in response to 12 weeks of resistance exercise training in older
830 adults. *Acta Physiologica* e13599, 2020.
- 831 50. **Eftestøl E, Egner IM, Lunde IG, Ellefsen S, Andersen T, Sjøland C, Gundersen K, and**
832 **Bruusgaard JC.** Increased hypertrophic response with increased mechanical load in skeletal muscles
833 receiving identical activity patterns. *American Journal of Physiology-Cell Physiology* 311: C616-C629,
834 2016.
- 835 51. **Vijayan K, Thompson JL, and Riley DA.** Sarcomere lesion damage occurs mainly in slow
836 fibers of reloaded rat adductor longus muscles. *Journal of Applied Physiology* 85: 1017-1023, 1998.
- 837 52. **Vijayan K, Thompson JL, Norenberg KM, Fitts R, and Riley DA.** Fiber-type susceptibility to
838 eccentric contraction-induced damage of hindlimb-unloaded rat AL muscles. *Journal of Applied*
839 *Physiology* 90: 770-776, 2001.
- 840 53. **Masschelein E, D'Hulst G, Zvick J, Hinte L, Soro-Arnaiz I, Gorski T, von Meyenn F, Bar-Nur**
841 **O, and De Bock K.** Exercise promotes satellite cell contribution to myofibers in a load-dependent
842 manner. *Skeletal Muscle* 10: 21, 2020.
- 843 54. **Smith HK, Maxwell L, Rodgers CD, McKee NH, and Plyley MJ.** Exercise-enhanced satellite
844 cell proliferation and new myonuclear accretion in rat skeletal muscle. *Journal of Applied Physiology*
845 90: 1407-1414, 2001.
- 846 55. **Cramer R, Aagaard P, Qvortrup K, Langberg H, Olesen J, and Kjær M.** Myofibre damage in
847 human skeletal muscle: effects of electrical stimulation versus voluntary contraction. *The Journal of*
848 *physiology* 583: 365-380, 2007.
- 849 56. **Ashley Z, Salmons S, Boncompagni S, Protasi F, Russold M, Lanmuller H, Mayr W,**
850 **Sutherland H, and Jarvis JC.** Effects of chronic electrical stimulation on long-term denervated
851 muscles of the rabbit hind limb. *Journal of Muscle Research and Cell Motility* 28: 203-217, 2007.
- 852 57. **Ashley Z, Sutherland H, Lanmuller H, Russold M, Unger E, Bijak M, Mayr W, Boncompagni**
853 **S, Protasi F, and Salmons S.** Atrophy, but not necrosis, in rabbit skeletal muscle denervated for
854 periods up to one year. *American Journal of Physiology-Cell Physiology* 292: C440-C451, 2007.
- 855 58. **Jackson JR, Mula J, Kirby TJ, Fry CS, Lee JD, Ubele MF, Campbell KS, McCarthy JJ, Peterson**
856 **CA, and Dupont-Versteegden EE.** Satellite cell depletion does not inhibit adult skeletal muscle
857 regrowth following unloading-induced atrophy. *American Journal of Physiology-Cell Physiology* 2012.
- 858 59. **Seaborne RA, Hughes DC, Turner DC, Owens DJ, Baehr LM, Gorski P, Semenova EA, Borisov**
859 **OV, Larin AK, and Popov DV.** UBR5 is a novel E3 ubiquitin ligase involved in skeletal muscle
860 hypertrophy and recovery from atrophy. *The Journal of physiology* 597: 3727-3749, 2019.

- 861 60. **Michel RN, and Gardiner PF.** To what extent is hindlimb suspension a model of disuse?
862 *Muscle & Nerve: Official Journal of the American Association of Electrodiagnostic Medicine* 13: 646-
863 653, 1990.
- 864 61. **Pierotti DJ, Roy RR, Flores V, and Edgerton V.** Influence of 7 days of hindlimb suspension
865 and intermittent weight support on rat muscle mechanical properties. *Aviation, space, and*
866 *environmental medicine* 61: 205-210, 1990.
- 867 62. **Cormery B, Pons F, Marini J-F, and Gardiner PF.** Myosin heavy chains in fibers of TTX-
868 paralyzed rat soleus and medial gastrocnemius muscles. *Journal of Applied Physiology* 88: 66-76,
869 2000.
- 870 63. **Salter A-CD, Richmond FJ, and Loeb GE.** Effects of muscle immobilization at different lengths
871 on tetrodotoxin-induced disuse atrophy. *IEEE Transactions on neural systems and rehabilitation*
872 *engineering* 11: 209-217, 2003.
- 873 64. **Martinov VN, and Njå A.** A microcapsule technique for long-term conduction block of the
874 sciatic nerve by tetrodotoxin. *Journal of neuroscience methods* 141: 199-205, 2005.
- 875 65. **Reid B, Martinov VN, Njå A, Lømo T, and Bewick GS.** Activity-dependent plasticity of
876 transmitter release from nerve terminals in rat fast and slow muscles. *Journal of Neuroscience* 23:
877 9340-9348, 2003.
- 878 66. **Baehr LM, West DW, Marcotte G, Marshall AG, De Sousa LG, Baar K, and Bodine SC.** Age-
879 related deficits in skeletal muscle recovery following disuse are associated with neuromuscular
880 junction instability and ER stress, not impaired protein synthesis. *Aging (Albany NY)* 8: 127, 2016.
- 881 67. **Baehr LM, West DW, Marshall AG, Marcotte GR, Baar K, and Bodine SC.** Muscle-specific
882 and age-related changes in protein synthesis and protein degradation in response to hindlimb
883 unloading in rats. *Journal of applied physiology* 122: 1336-1350, 2017.

884

885 Figure Legends:

886 Figure 1: Schematic representation of electrical stimulation experimental time courses studied and timepoints of
887 euthanasia and muscle harvest. For electrical stimulation experiments, an implantable pulse generator (IPG) was placed
888 within the abdomen with electrodes leading subcutaneously to the left hindlimb with one of two electrode placements.
889 Either with the anode placed under the tibial nerve and the cathode under the common peroneal nerve (CPN) to produce
890 Spillover (loaded) resistance exercise of the tibialis anterior or with both electrodes under the CPN to elicit concentric
891 (unloaded) resistance exercise or continuous low frequency stimulation to elicit endurance training).

892 Figure 2: An overview of the in-situ placement of the osmotic pump loaded with a pre-determined volume of tetrodotoxin
893 (TTX), placed in the scapula region with silicone tubing leading to the left hind-limb and the silicone cuff that encircled the
894 common peroneal nerve (CPN) to selectively block the ankle dorsiflexors, while maintaining normal plantarflexion.

895 Figure 3: Control tibialis anterior (TA) muscles. (A) Fiber type distribution, (B) Muscle fiber cross-sectional area, (C)
896 Myonuclei per fiber cross-section, (D) Myonuclear domain size. $n = 32$. (E) Total number of muscle fibers detected per mid-
897 belly transverse cross-section. $n = 64$. (F) Total number of muscle fibers detected between experimental condition groups
898 and their contralateral control limb. Note spread of control values in each group and small differences between left and
899 right limbs. $*P \leq 0.05$. $**P \leq 0.01$. $***P \leq 0.001$. $****P \leq 0.0001$. Mean \pm Standard Deviation. (G) Example hematoxylin and
900 eosin staining of TA mid-belly cross-section following 14 days of TTX treatment for assessment of damage, degeneration,
901 and denervation. (H) Serial immunofluorescence section of G, depicting the deep oxidative portion toward the top right of
902 the transverse section (More green and red fibers). (Magenta = Dystrophin, Blue = Nuclei, Green = Type 1, Red = Type IIA,
903 Black Fibers = Type IIX/IIB). Scale bar = 2000 μ m. (I) Higher magnification of muscle fiber staining from deep oxidative
904 portion. Scale bar = 40 μ m.

905 Figure 4: changes in response to 7 days low frequency continuous stimulation: (A) Percentage change in muscle mass
906 between the left experimental tibialis anterior (TA) and right contralateral control TA, 7 days after sham surgery or after 7
907 days of continuous 24-hour low-frequency stimulation (CLFS). (B-D) Fiber CSA, myonuclei per fiber cross-section and
908 myonuclear domain size assessed across all muscle fibers, expressed as percentage change between left experimental TA
909 and right contralateral control TA for the same groups as in (A). (E-G) Fiber type proportions in control and after 7 days of
910 low frequency stimulation. (H-J) Fiber type-specific fiber CSA. (K-M) Fiber type specific myonuclei per fiber cross-section
911 measurements. (N-P) Fiber type specific myonuclear domain sizes. $*P \leq 0.05$. $**P \leq 0.01$. $***P \leq 0.001$. $****P \leq 0.0001$.
912 Mean \pm Standard Deviation.

913 Figure 5: (A) Percentage change in muscle mass relative to body mass between the left experimental tibialis anterior (TA)
914 and right contralateral control TA, over a time course (2d, 10d, 20d, 30d) of Spillover(loaded) training or 30d of unloaded

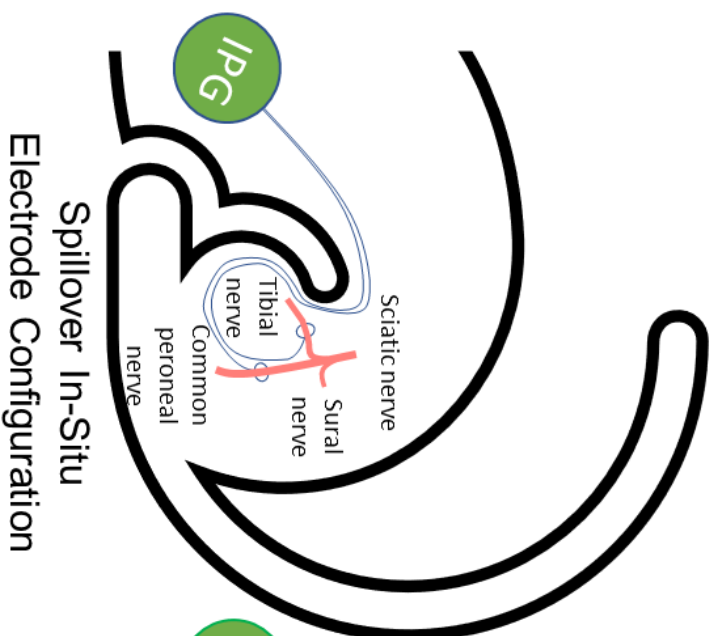
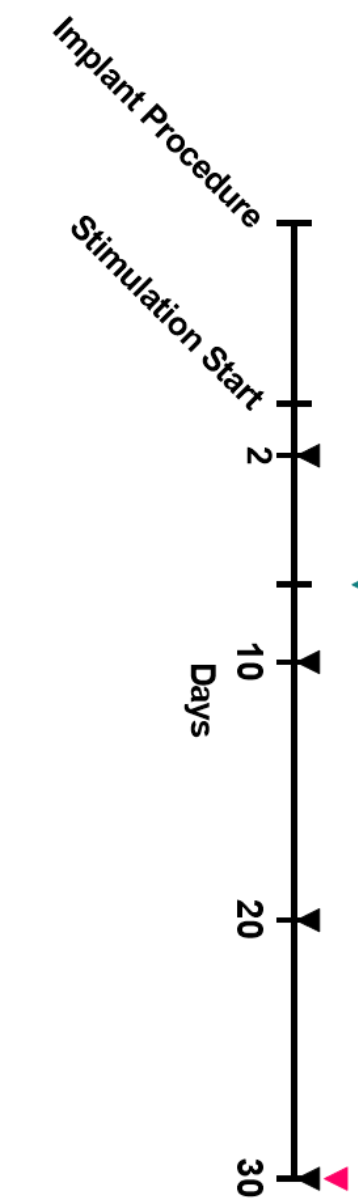
915 resistance training. (B-D) Fiber CSA, myonuclei per fiber cross-section and myonuclear domain size assessed across all
916 muscle fibers, expressed as percentage change between left experimental TA and right contralateral control TA. (E-G) Fiber
917 type proportions in control, 30 days loaded resistance training and 30 days unloaded training. (H-J) Fiber type specific fiber
918 CSA. (K-M) Fiber type specific myonuclei per fiber cross-section measurements. (N-P) Fiber type-specific myonuclear
919 domain sizes. *P ≤ 0.05. **P ≤ 0.01. ***P ≤ 0.001. ****P ≤ 0.0001. Mean ± Standard Deviation.

920 Figure 6: (A) Percentage change in muscle mass between the left experimental tibialis anterior (TA) and right contralateral
921 control TA, over a time course (3d, 7d, 14d) of tetrodotoxin (TTX)-induced nerve silencing atrophy and subsequent
922 recovery through 7d habitual activity. (B-D) Fiber CSA, myonuclei per fiber cross-section and myonuclear domain size
923 assessed across all muscle fibers, expressed as percentage change between left experimental TA and right contralateral
924 control TA. (E-G) Fiber type proportions in control, following 14 days atrophy and following 14 days of atrophy with 7 days
925 of subsequent recovery. (H-J) Fiber type-specific fiber CSA. (K-M) Fiber type-specific myonuclei per fiber cross-section
926 measurements. (N-P) Fiber type-specific myonuclear domain sizes. *P ≤ 0.05. **P ≤ 0.01. ***P ≤ 0.001. ****P ≤ 0.0001.
927 Mean ± Standard Deviation.

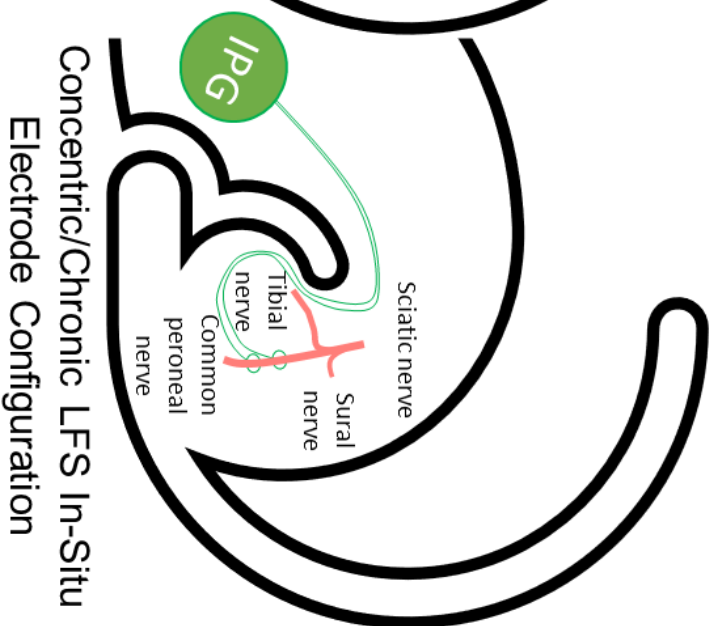
928 Figure 7: (A-F) Correlations between percentage changes in muscle mass, muscle fiber CSA, myonuclei per fiber cross-
929 section and myonuclear domain size following a time course of loaded and unloaded resistance training. (G-L) Correlations
930 between percentage changes in muscle mass, muscle fiber CSA, myonuclei per fiber cross-section and myonuclear domain
931 size following a time course of TTX-induced atrophy. The subsequent 7-day recovery following 14 days of TTX induced
932 atrophy is expressed as the difference between the mean 14 days TTX value versus the individual 7-day recovery values.

Electrical Stimulation Experiments

- ▼ Euthanasia Following Daily 'Spillover' Training
- ▼ Euthanasia Following Daily Concentric Training
- ▼ Euthanasia Following 20Hz Chronic Stimulation



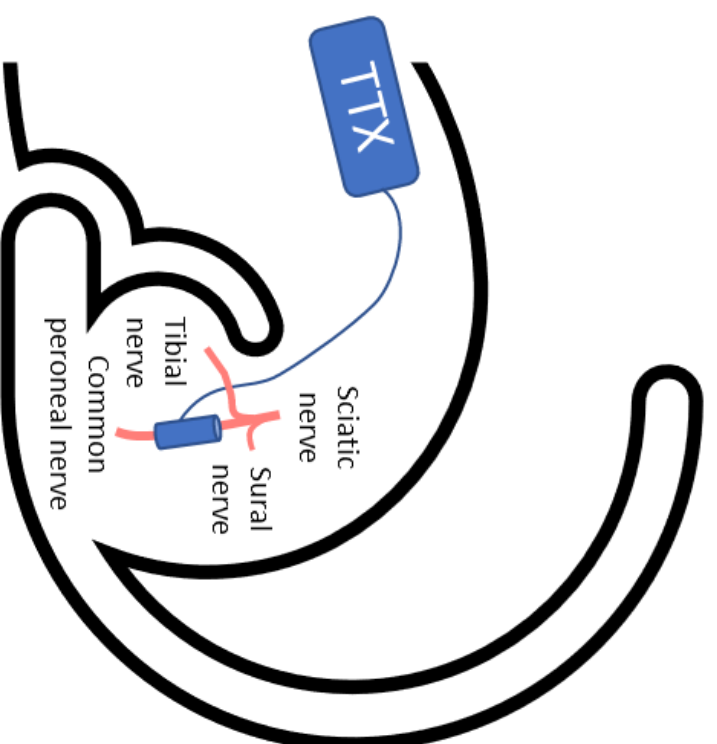
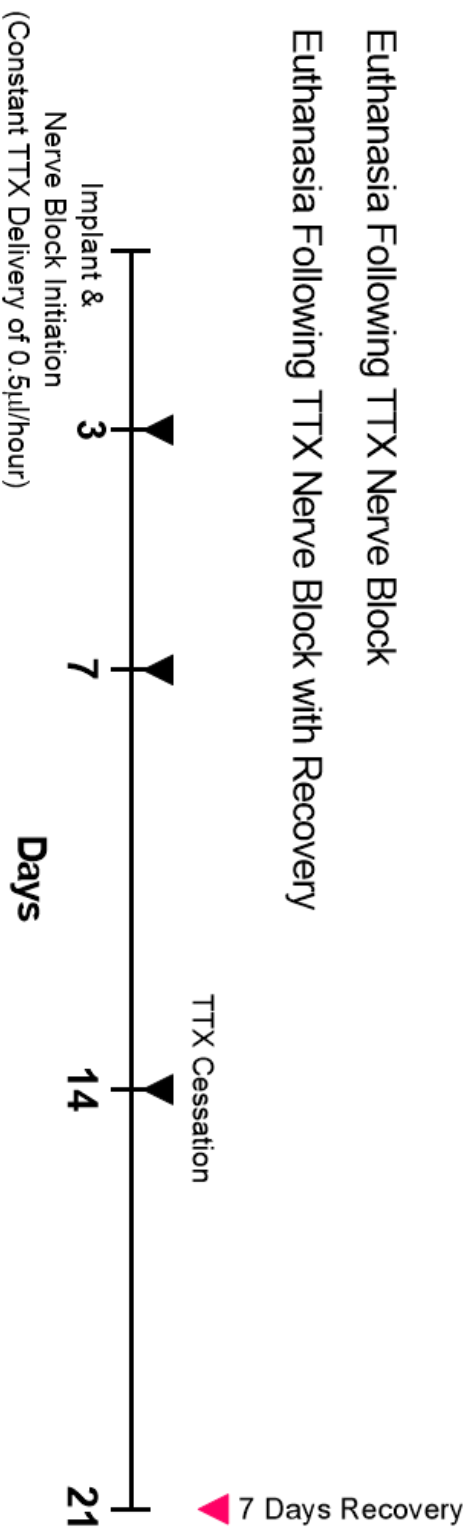
Spillover In-Situ
Electrode Configuration

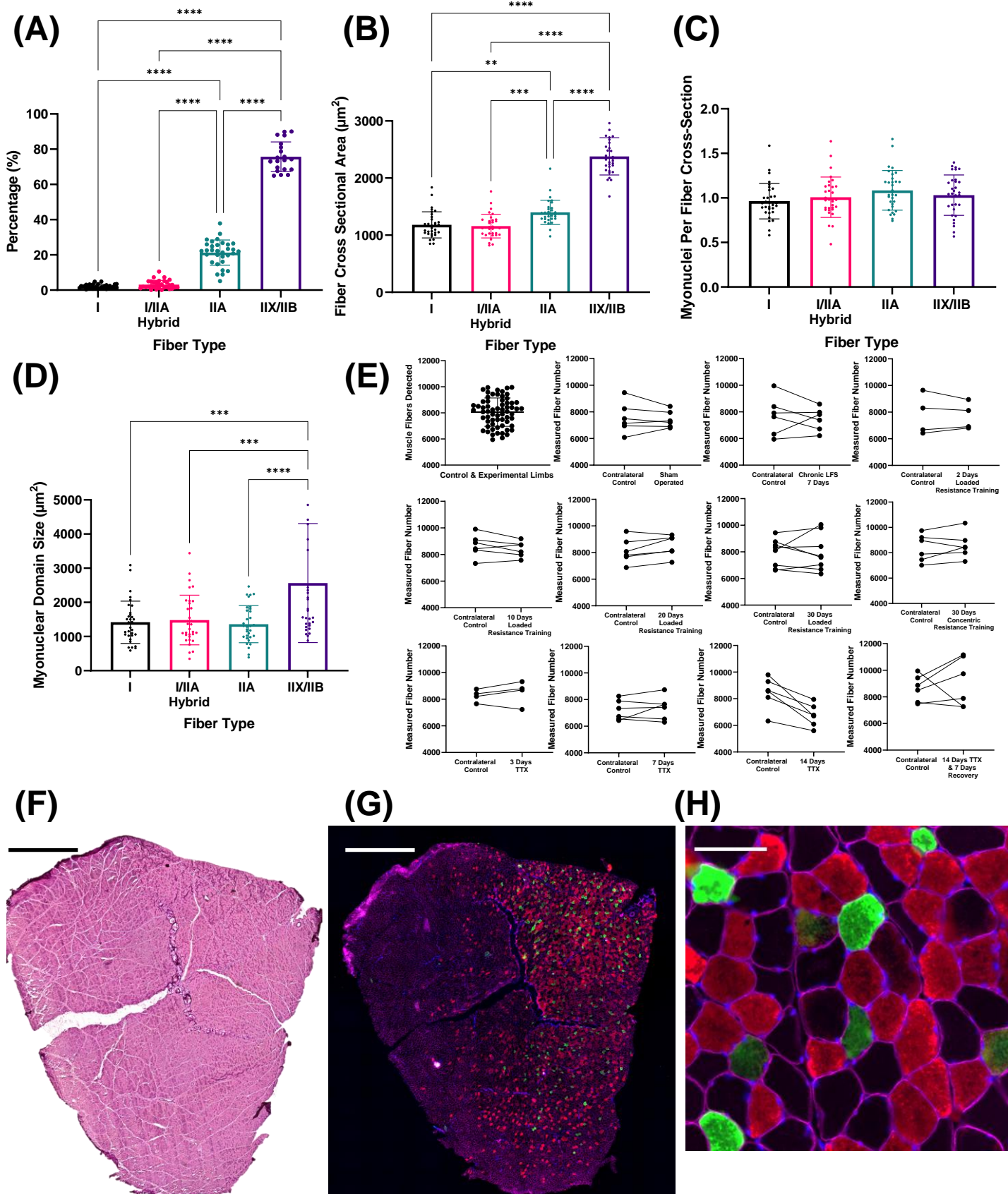


Concentric/Chronic LFS In-Situ
Electrode Configuration

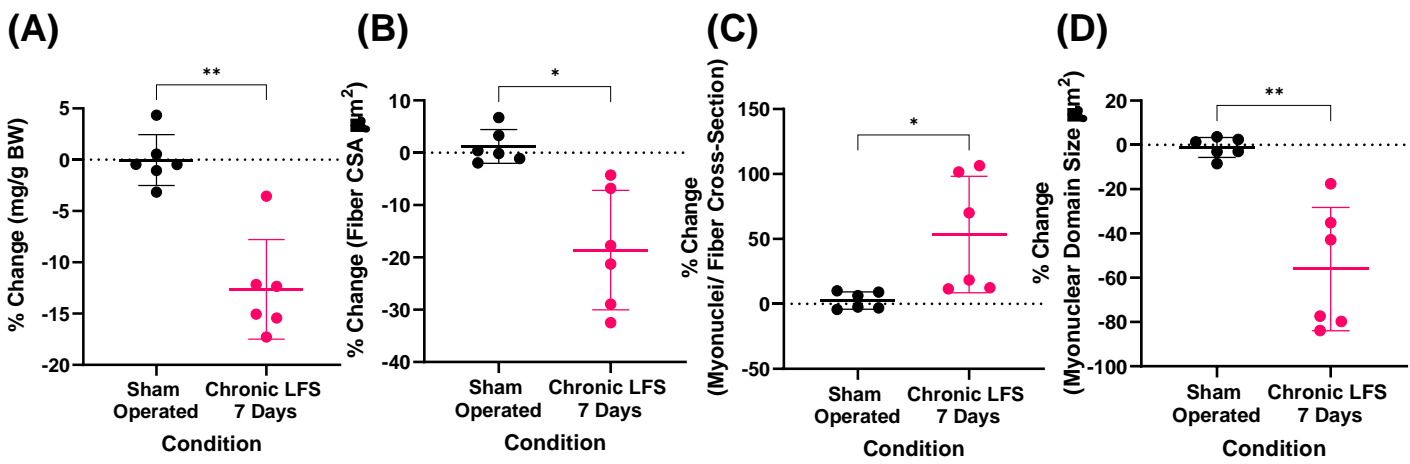
Nerve Silencing Experiments

- ▼ Euthanasia Following TTX Nerve Block
- ▼ Euthanasia Following TTX Nerve Block with Recovery

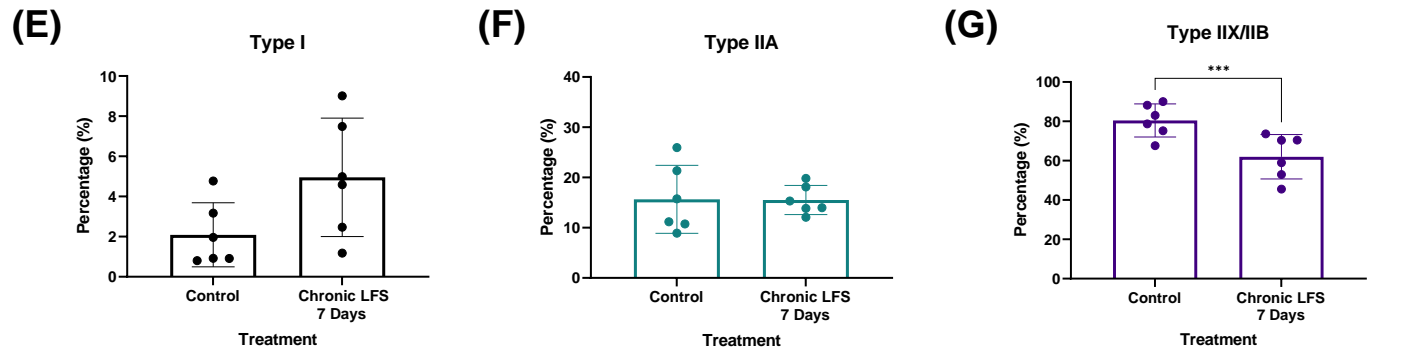




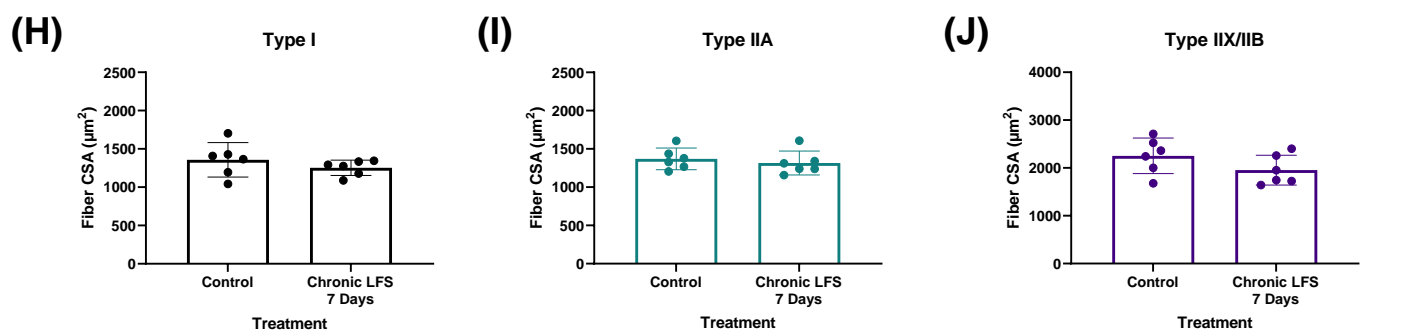
Response to 7 days continuous, low frequency stimulation (20Hz)



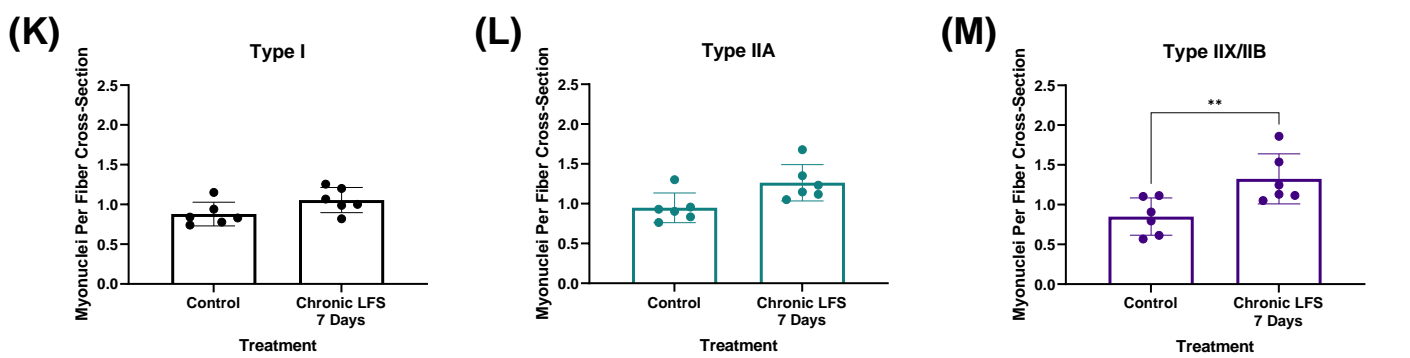
Fiber Type Percentages



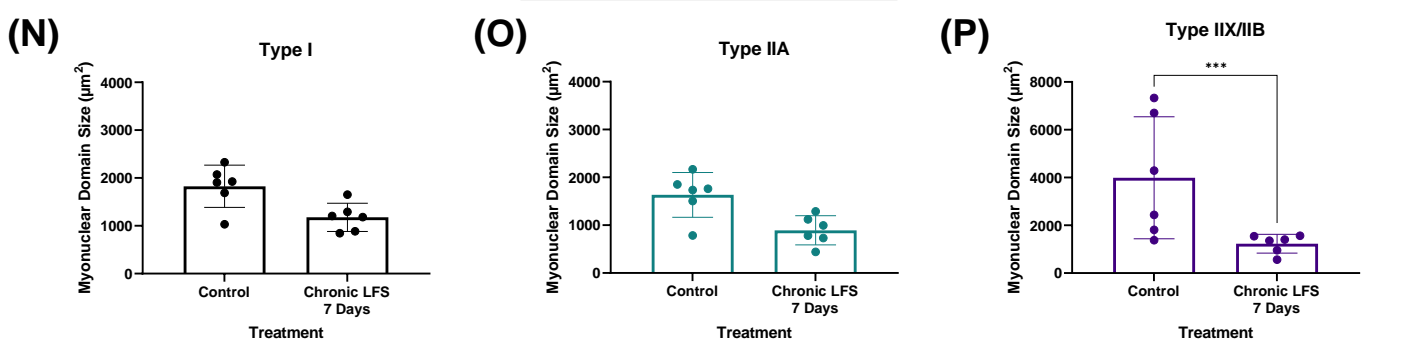
Fiber Area



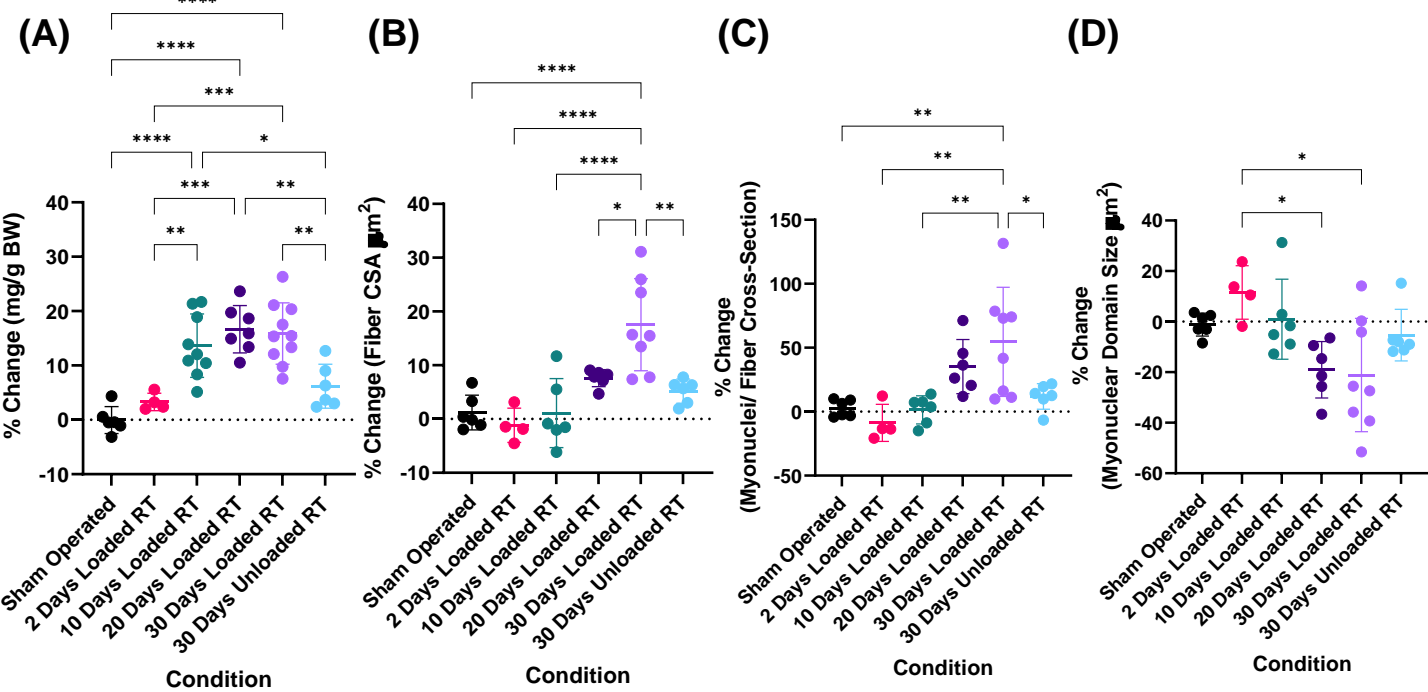
Myonuclei Per Fiber Cross-section



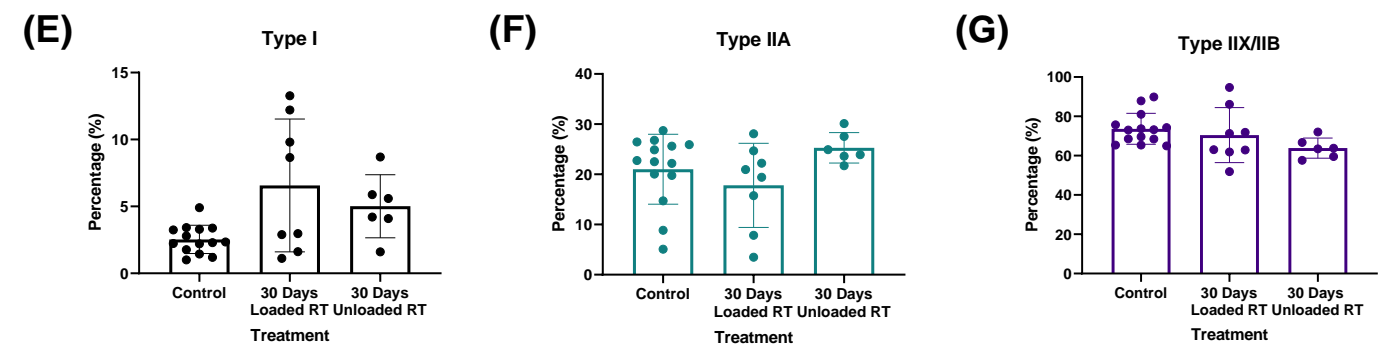
Myonuclear Domain Size



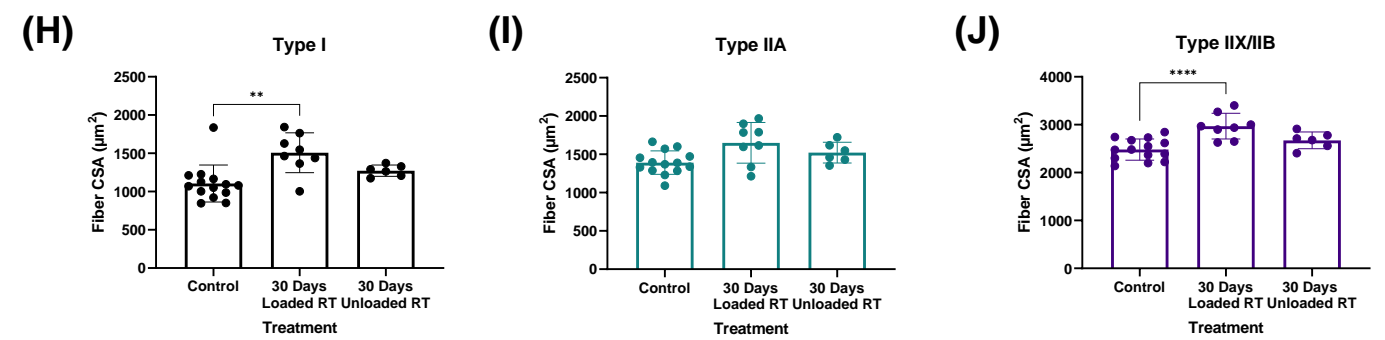
Time course response to loaded & unloaded resistance training



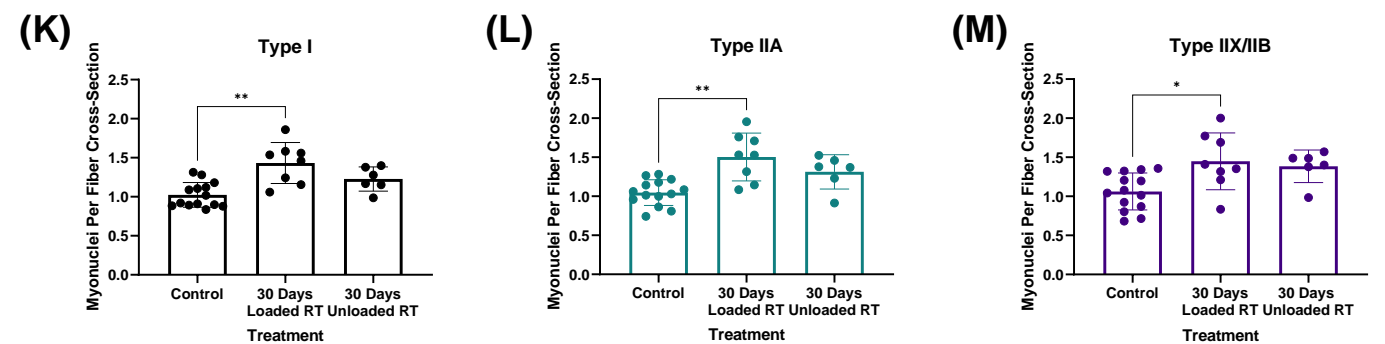
Fiber type percentages following 30 days of loaded and unloaded resistance training



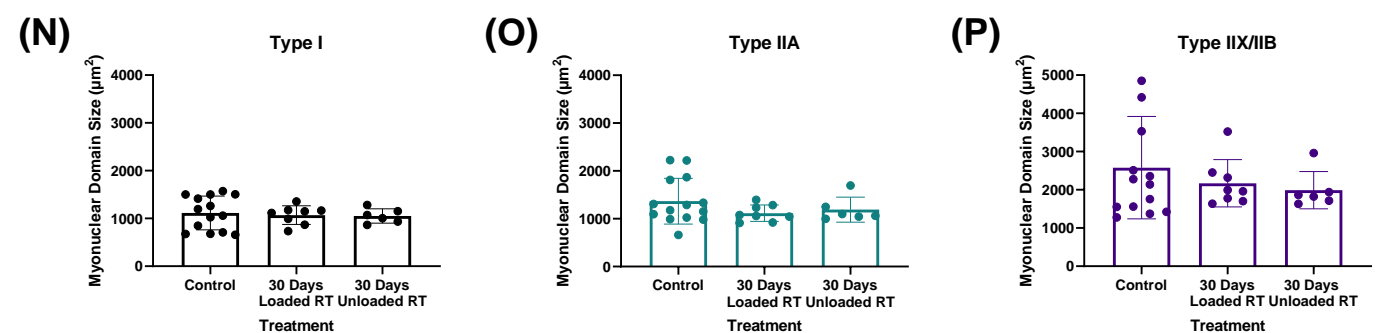
Fiber area following 30 days of loaded and unloaded resistance training



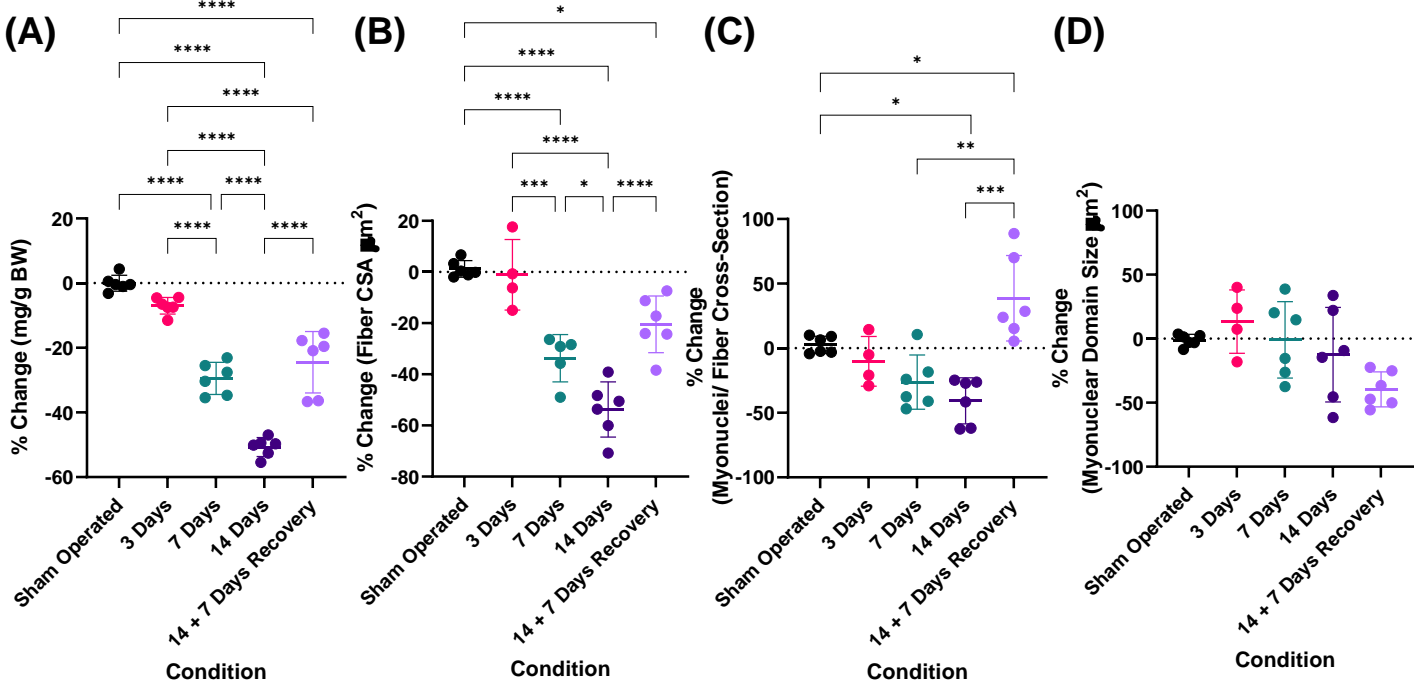
Myonuclei per fiber cross-section following 30 days of loaded and unloaded resistance training



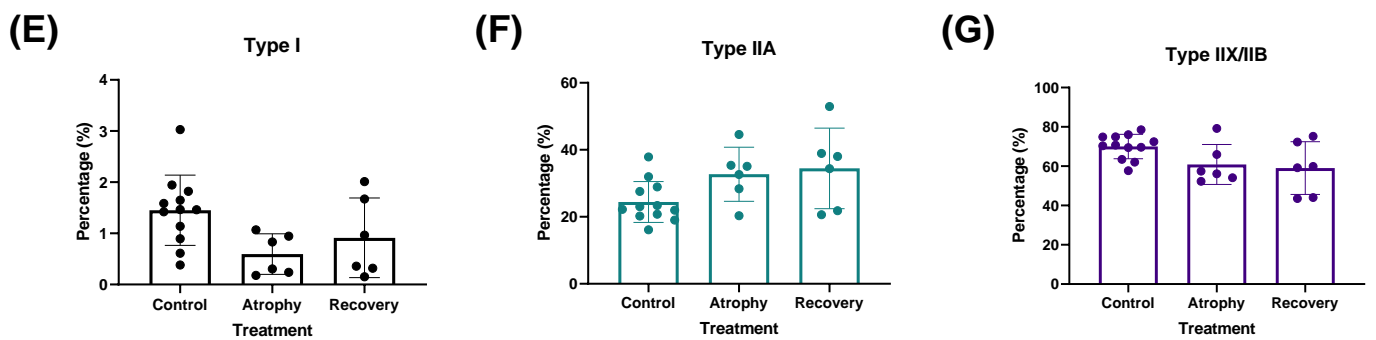
Myonuclear domain size following 30 days of loaded and unloaded resistance training



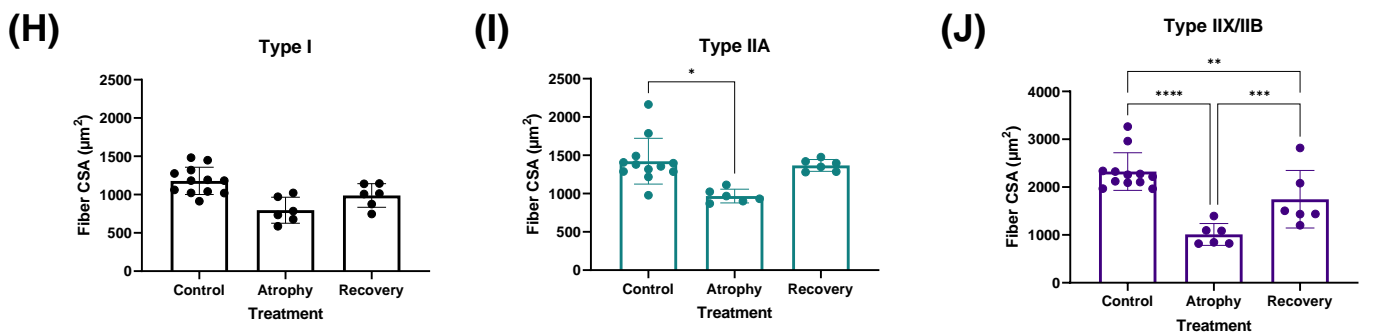
Time course response to TTX-induced atrophy and recovery



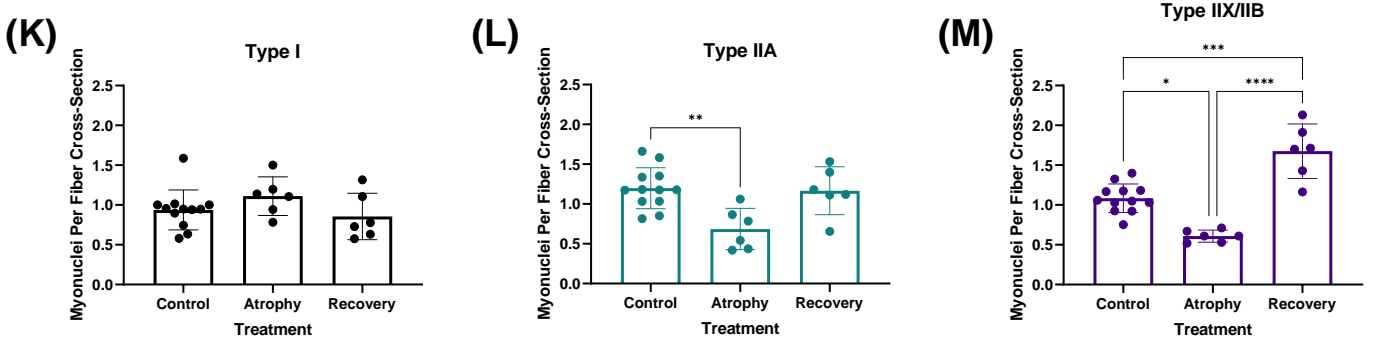
Fiber type percentages in disuse atrophy and recovery



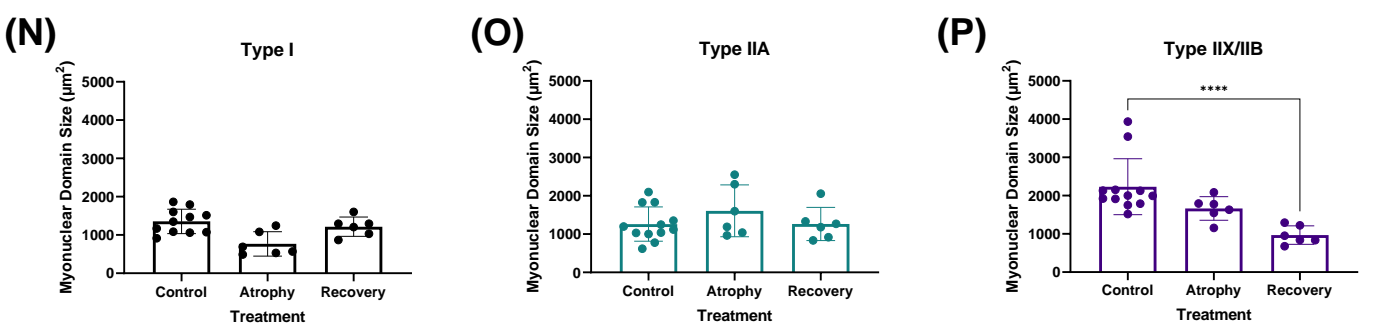
Fiber area in disuse atrophy and recovery



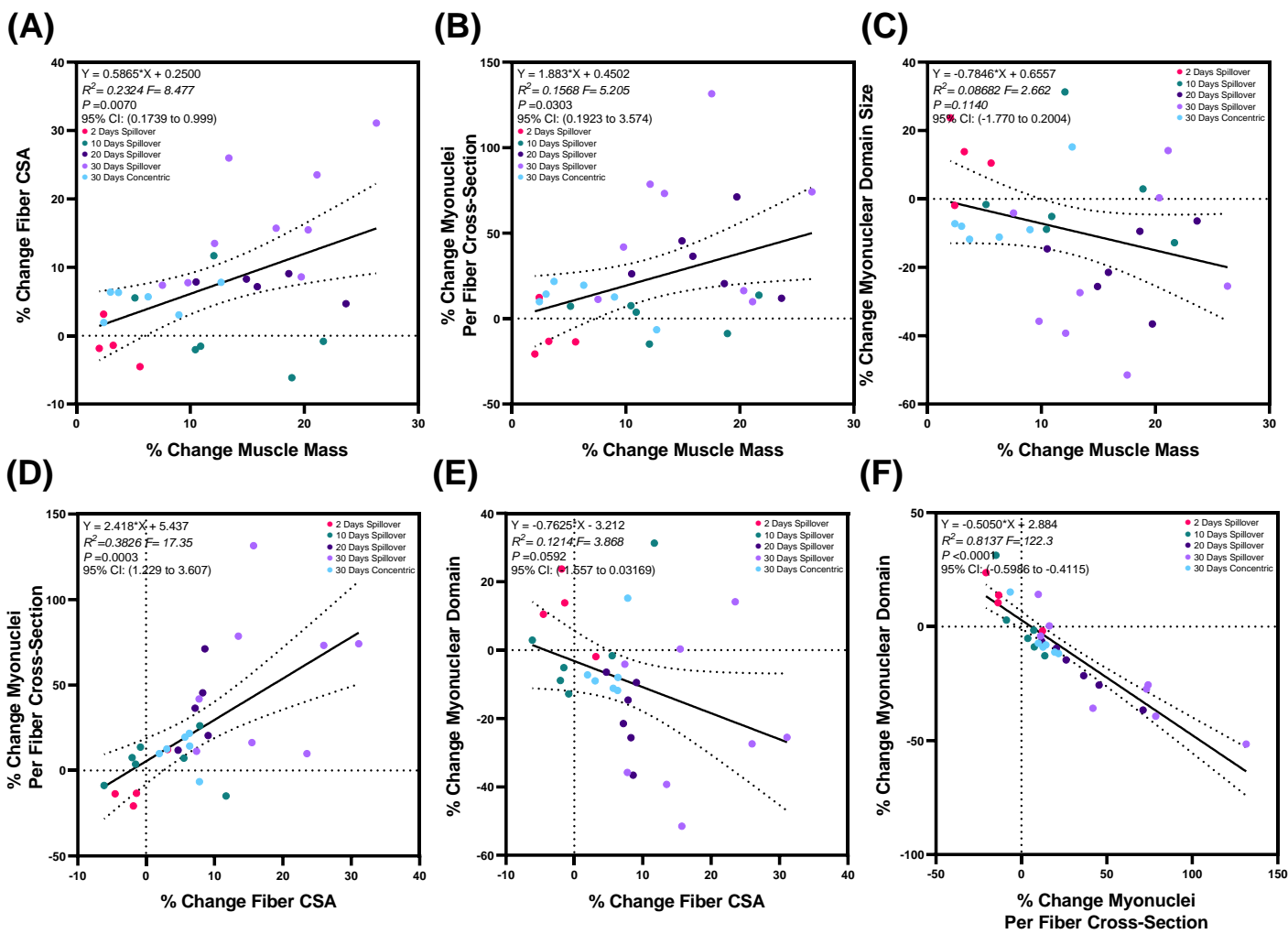
Myonuclei per fiber cross-section in disuse atrophy and recovery



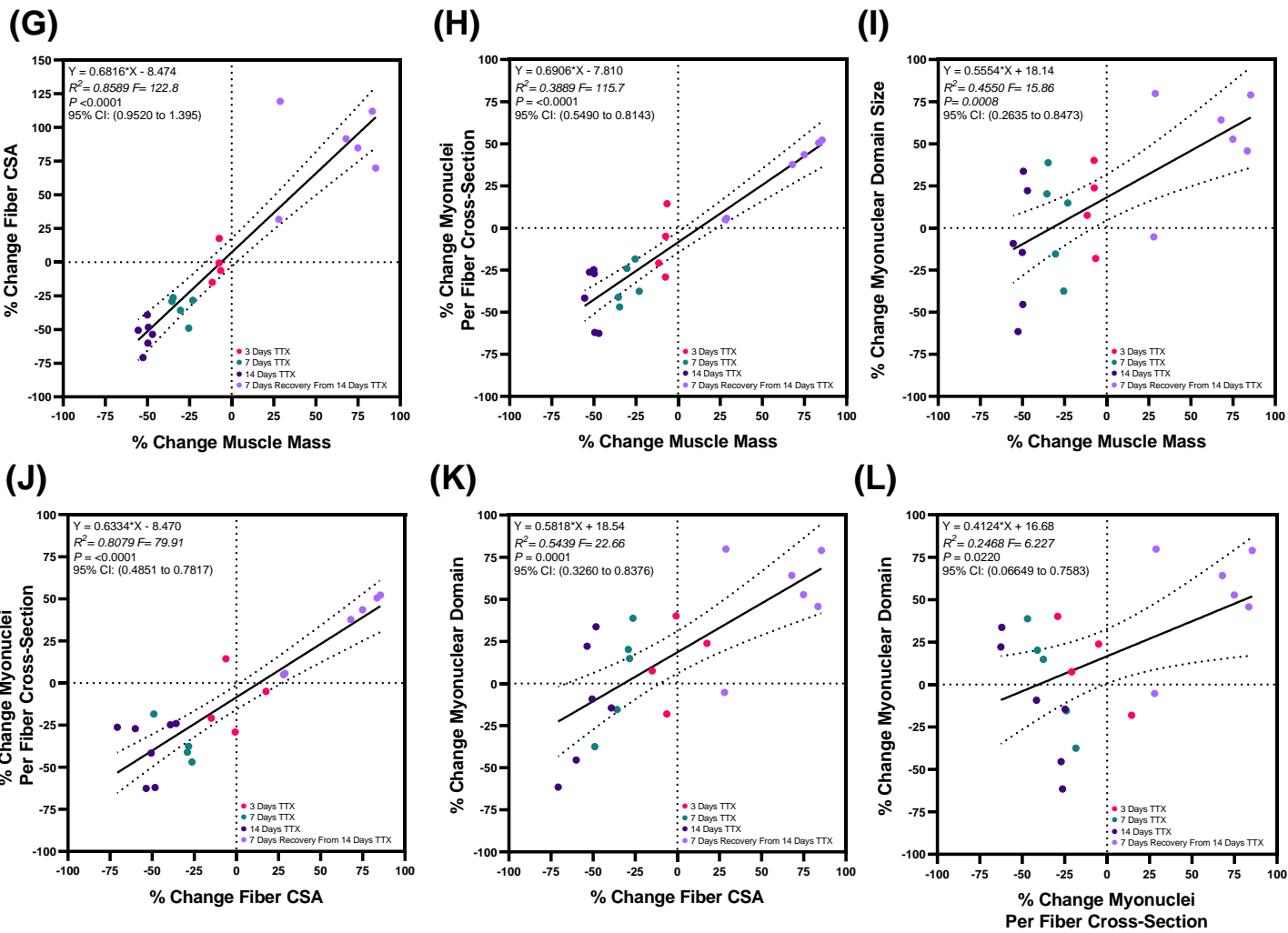
Myonuclear domain size in disuse atrophy and recovery



Correlations between adaptive responses to electrical stimulation-induced resistance training



Correlations between adaptive responses to TTX induced atrophy and subsequent recovery



Primary Ab	Secondary Ab
MANDYS8(8H11) (Anti-dystrophin) DSHB Supernatant. Morris, G.E. (Developmental Studies Hybridoma Bank (DSHB) Hybridoma Product)	Goat anti-mouse IgG H&L (AlexaFluor® 594) preadsorbed Abcam (Cambridge, UK) (ab150120)
Dystrophin Polyclonal Antibody. Catalog #PA5-32388. (Thermofisher Scientific)	Goat anti-Rabbit IgG (H+L) Cross-Adsorbed Secondary Antibody, Alexa Fluor 633. A-21070 (Thermofisher Scientific)
BA-D5 (anti type I myosin) DSHB Supernatant. Schiaffino, S. (DSHB Hybridoma Product)	Goat anti-Mouse IgG2b Cross-Adsorbed Secondary Antibody, Alexa Fluor 488. A-21141 (Thermofisher Scientific)
SC-71 (anti type IIA myosin) DSHB Supernatant. Schiaffino, S. (DSHB Hybridoma Product)	Goat anti-Mouse IgG1 Cross-Adsorbed Secondary Antibody, Alexa Fluor 546. A-21123 (Thermofisher Scientific)

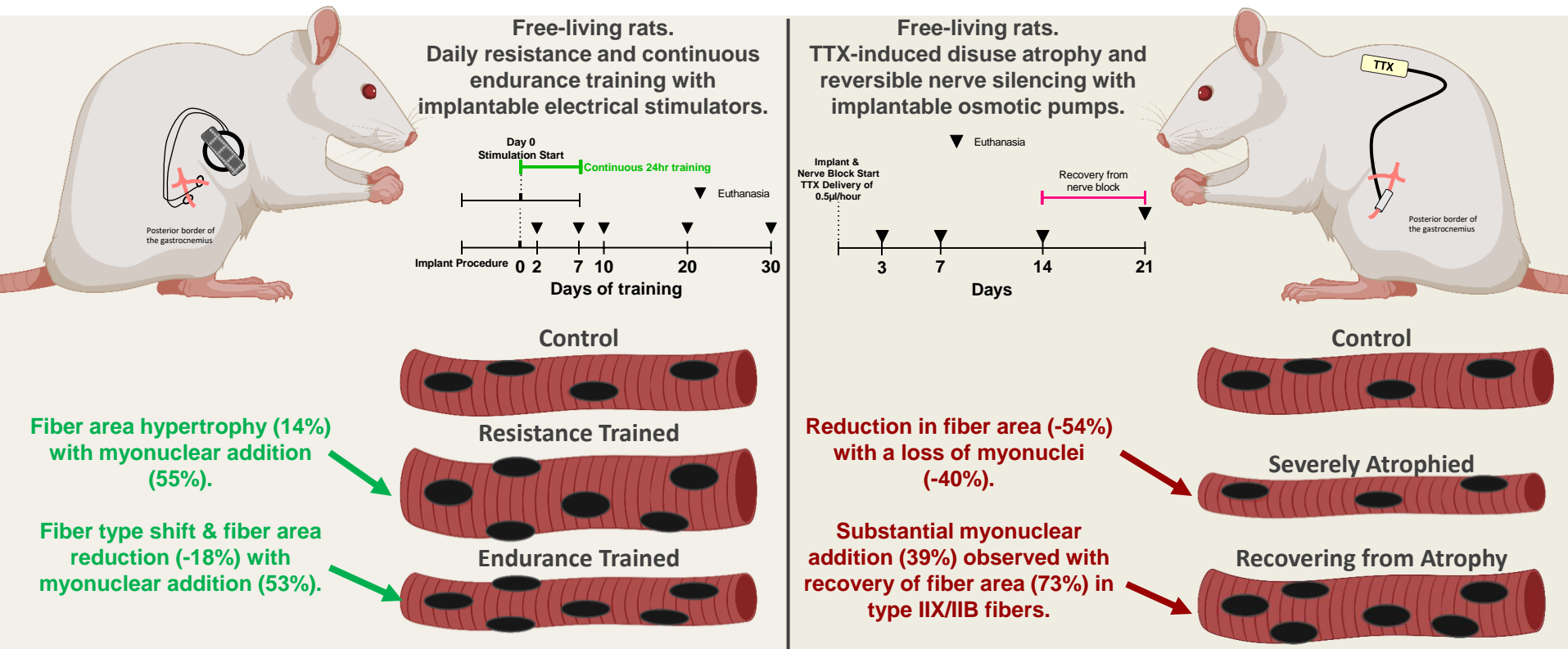
Table 1: Primary antibodies and appropriate corresponding secondary antibodies used.

Table 2: Body weight pre-surgery and post intervention for each experimental group.

Condition	Pre-Surgical Weight (M ± SD)	Post-Intervention Weight (M ± SD)
Sham Operated	443 ± 31	484 ± 78
CLFS 7 Days	397 ± 17	400 ± 20
2 Days Spillover	419 ± 58	411 ± 55
10 Days Spillover	382 ± 47	401 ± 52
20 Days Spillover	372 ± 34	416 ± 30
30 Days Spillover	413 ± 38	472 ± 52
30 Days Concentric	396 ± 33	415 ± 31
3 Days TTX	390 ± 12	416 ± 14
7 Days TTX	387 ± 22	420 ± 18
14 Days TTX	378 ± 11	417 ± 25
14 Days TTX + 7 Days Recovery	403 ± 35	452 ± 25

Mean	398	428
SD	20	27

Automated cross-sectional analysis of trained, severely atrophied and recovering rat skeletal muscles using MyoVision 2.0



CONCLUSION: Myonuclei number per unit fiber length is not fixed and does not always correlate with fiber size. Myonuclear density appears to reflect the changes in activation and loading of the muscle fiber. Type IIX/IIB fibers show greater plasticity than slower types.